Spatiotemporal Changes in Netrin/Dscam1 Signaling Dictate Axonal Projection Direction in *Drosophila* Small Ventral Lateral Clock Neurons

Jingjing Liu[1], Yuedong Wang[1], Junhai Han[1,2,*], Yao Tian[1,*]

[1] School of Life Science and Technology, the Key Laboratory of Developmental Genes and Human Disease, Southeast University, Nanjing 210096, China

[2] Co-innovation Center of Neuroregeneration, Nantong University, Nantong, China

* Correspondence: junhaihan@seu.edu.cn, yaotian@seu.edu.cn,

Abstract

Axon projection is a spatial and temporal-specific process in which the growth cone receives environmental signals guiding axons to their final destination. However, the mechanisms underlying changes in axonal projection direction without well-defined landmarks remain elusive. Here, we present evidence showcasing the dynamic nature of axonal projections in *Drosophila*'s small ventral lateral clock neurons (s-LNvs). Our findings reveal that these axons undergo an initial vertical projection in the early larval stage, followed by a subsequent transition to a horizontal projection in the early-to-mid third instar larvae. The vertical projection of s-LNv axons correlates with mushroom body calyx expansion, while the s-LNv-expressed Down syndrome cell adhesion molecule (Dscam1) interacts with Netrins to regulate the horizontal projection. During a specific temporal window, locally newborn dorsal clock neurons (DNs) secrete Netrins, facilitating the transition of axonal projection direction in s-LNvs. Our study establishes a compelling *in vivo* model to probe the mechanisms of axonal projection direction switching in the absence of clear landmarks. These findings underscore the significance of dynamic local microenvironments in the synergetic regulation of axonal projection direction transitions.

Keywords: Axon projection; projection direction switch; Dscam1; Netrin; s-LNvs; *Drosophila*;

Introduction

During nervous system development, neurons extend axons to reach their targets in order to build functional neural circuits (Cang & Feldheim, 2013; Kaas, 1997). The growth cone, which is specialized at the tip of the extending axon, is critical for receiving multiple guidance signals from the external environment to guide axon projection (Lowery & Vactor, 2009; Mortimer et al., 2008; Vitriol & Zheng, 2012). Guidance cues regulate cytoskeletal dynamics through growth cone-specific receptors, steering axons via attractive or repulsive signals (Araújo & Tear, 2003; Koch et al., 2012; Kolodkin & Tessier-Lavigne, 2011; Esther T Stoeckli, 2018; Zang et al., 2021). Over the last 30 years, several guidance cues have been identified and divided into four classical families: Semaphorins, Ephrins, Netrins, and Slits (Derijck et al., 2010; Dickson, 2002; Goodhill, 2016; X.-T. Li et al., 2014; Orioli & Klein, 1997). The emergence of other kinds of guidance cues, including morphogens, growth factors, and cell adhesion molecules, increases the complexity of axon pathfinding (Chan & Odde, 2008; Chédotal et al., 2012; Kahn & Baas, 2016; Vitriol & Zheng, 2012).

When going through a long-distance pathfinding process in the complex and highly dynamic *in vivo* environment, axons frequently undergo multiple changes in their projection directions (Squarzoni et al., 2015). Crucially, intermediate targets play a pivotal role by providing vital guiding information that enables axons to transition their projection directions and embark upon the subsequent stages of their journey, ultimately leading them to their final destination (de Ramon Francàs et al., 2017; Garel & Rubenstein, 2004; Squarzoni et al., 2015). Certain intermediate targets can respond to the growth cone's signaling to maintain a dynamic balance between attractive and repulsive forces(Bron et al., 2007; Martins et al., 2022). One of the well-studied intermediate target projection types is the midline cross model (Derijck et al., 2010; Yang et al., 2009). As a clear landmark, axons need to project to the midline first and then leave it immediately (Gorla & Bashaw, 2020; Neuhaus-Follini & Bashaw, 2015). The midline floor plate cells secreted long-range attractive signals to attract commissural axons towards them (Kennedy et al., 1994; Serafini et al., 1996). Once there, these cells emit signals of rejection to prevent excessive closeness of axons, thus aiding the axon in departing the floor plate to reach its intended destination (Kidd et al., 1998; Long et al., 2004; E T Stoeckli et al., 1997). Comparatively, the

typical axonal projection process within the *in vivo* milieu undergoes multiple transitions in projection direction without a distinct landmark, such as the midline (Garel & López-Bendito, 2014; Gezelius & López-Bendito, 2017). However, how the axons change their projection direction without well-defined landmarks is still unclear.

Drosophila small ventral lateral clock neurons (s-LNvs) exhibit the typical tangential projection pattern in the central brain (Agrawal & Hardin, 2016; Gummadova et al., 2009; Hardin, 2017; Helfrich-Förster, 1997). The s-LNv axons originate from the ventrolateral soma and project to the dorsolateral area of the brain, and subsequently undergo a axon projection direction shift, projecting horizontally toward the midline with a short dorsal extension (Helfrich-Förster et al., 2007). Several studies have reported the impact of various factors, including the Slit-Robo signal (Oliva et al., 2016), Lar (leukocyte-antigen-related) (Agrawal & Hardin, 2016), dfmr1 (Okray et al., 2015), dTip60 (Pirooznia et al., 2012), and Dscam1 long 3' UTR (Zhang et al., 2019), on the axon outgrowth of s-LNvs in the adult flies' dorsal projection. However, the mechanism underlying the projection direction switch of s-LNv axons remains largely unknown. Here, we show that s-LNvs and newborn dorsal clock neurons (DNs) generate spatiotemporal-specific guidance cues to precisely regulate the transition of projection direction in s-LNv axons. This regulation uncovers unexpected interdependencies between axons and local microenvironment dynamics during the navigation process, enabling accurate control over axon projection.

Results

s-LNvs axons change their projection direction in the early-to-mid third instar larvae

The stereotypical trajectory of the s-LNvs axon projection can be succinctly characterized as an initial vertical extension originating from the ventrolateral brain, followed by a directional pivot at the dorsolateral protocerebrum, ultimately leading to a horizontal projection towards the midline. Immunoreactivity for pigment-dispersing factor (PDF) (Cyran et al., 2005), representing the pattern of LNv neurons, is initially detected in the brains of 1st-instar larvae 4-5 hours after larval hatching (ALH) (Helfrich-Förster, 1997). To elucidate the intricate axon pathfinding process during development, we employed a dual-copy *Pdf-GAL4* to drive the expression of double-copy UAS-mCD8::GFP, visualizing the s-LNvs at the larval stage (Figure 1A). At 8 hours ALH, the

GFP signal strongly co-localized with the PDF signal within the axons. This remarkable co-localization continued throughout the larval stage, particularly concentrated at the axon's terminal end (Figure 1A).

We then quantified the process of s-LNvs axonal projection. The vertical projection distance of the s-LNvs axon was ascertained by measuring the vertical span between the lowest point of the optical lobe and the highest point of the axon's projection terminal. Statistical analyses revealed a steadfast linear increase in the vertical projection distance of the s-LNvs axon as larval development progressed (Figure 1A-B). To determine the horizontal projection distance of the s-LNvs axon, we applied the methodology employed by Olive *et al.* for measuring adult flies (Oliva et al., 2016). A tangent line is drawn precisely at the pivotal juncture where the s-LNvs axon undergoes a shift in its projection direction. We define the Arbitrary Unit (A.U.) as the ratio between the horizontal distances from this point to both the end of the axon projection and the midline (Figure 1A and 1C). Remarkably, at the time points of 8, 24, 48, and 72 hours ALH, the A.U. value for s-LNvs axon projection in the horizontal direction remained relatively stable at approximately 0.13. However, at 96 and 120 hours ALH, a significant and striking increase in the A.U. value ensued, eventually reaching approximately 0.25 (Figure 1C). These findings suggest that the precise transition of s-LNv axon projection from vertical towards the horizontal direction occurs in the early-to-mid third instar larvae, specifically during 72 to 96 hours ALH (Figure 1D).

Vertical projection of s-LNvs axons correlate with mushroom body calyx expansion

The axons of s-LNv project dorsally, coming in close proximity to the dendritic tree of the mushroom body (MB), specifically the calyx (Figures 2A and 2C). This spatial arrangement facilitates potential interactions between the s-LNvs axon and the MB. MB predominantly comprises 2500 intrinsic neurons, known as Kenyon Cells (KCs) (Puñal et al., 2021). The development of the MB is a dynamic process characterized by three primary types of KCs: α/β, α'/β', and γ, each following distinct temporal schedules of birth. The γ cells emerge from the embryonic stage until early 3rd-instar larval phase, while the α'/β' cells are born during the latter half of larval life, and the α/β cells appear in the post-larval stage (Lee et al., 1999; Puñal et al., 2021). We noticed that s-LNv axons exhibit only vertical growth before early 3rd-instar larval

stage, which coincides with the emergence of γ KCs. Consequently, we have contemplated the potential correlation between the vertical projection of s-LNv axons and the growth of the mushroom body.

Next, we closely monitored the spatial relationship between the calyx and the axon projections of the s-LNvs throughout different larval developmental stages (Figure 2A). We used *OK107-GAL4* and *Tab2-201Y-GAL4* to drive the expression of mCD8::GFP in all KC subtypes or specifically in γ KCs (Pauls et al., 2010), respectively, to visualize MB KCs. As development progressed, the calyx area defined by both GAL4 drivers exhibited a consistent expansion. Statistical analyses further confirmed that the calyx area increased proportionally with the advancement of developmental time, demonstrating a linear relationship (Figure 2B-C). Additionally, Pearson correlation analysis unveiled a robust positive correlation between the calyx area and the vertical projection distance of s-LNvs axon (r = 0.9987, $P < 0.0001$ for *OK107-GAL4*; r = 0.9963, P = *0.0003* for *Tab2-201Y-GAL4*) (Figure 2B-C). These compelling observations suggest that the MB calyx, and potentially specifically the calyx of γ KCs, exert significant influence on the vertical projection of the s-LNvs axon.

To validate our idea, we employed a straightforward approach to evaluate any changes in s-LNvs axon projection after ablating γ KCs using the apoptosis-promoting factors RPRC and HID driven by the *Tab2-201Y GAL4*. Initially, we confirmed the effectiveness of our approach. In the control group, the GFP signal in γ KCs remained unchanged, while the ablation group showed a significant reduction or complete absence of the signal (Figure 2-figure supplement 1). Subsequently, we examined the axon projection of s-LNvs under these conditions. In the non-ablated group, the vertical distance increased linearly during development, following the expected pattern (Figure 2D-E). However, in the ablation group, although the initial vertical projection of s-LNvs appeared normal, there was a noticeable decrease in vertical projection distance at 48 hours ALH. This vertical development trend ceased thereafter, with the vertical projection distance measuring only 20 to 30 μm at 72 hours ALH (Figure 2D-E). Importantly, in later larval stages, we observed that s-LNvs in certain larvae became undetectable (data not shown), suggesting the potential occurrence of apoptosis in these neurons following MB ablation.

These results underscore a significant association between MB development, specifically the γ KCs, and the vertical projection dynamics of s-LNv axons.

s-LNv-expressed Dscam1 mediate s-LNv axons horizontal projection

To decipher the signaling pathways governing s-LNvs axon horizontal projection, we performed a screening with a total of 285 targets by using the RNA-interfering (RNAi) approach (Supplementary File 3). To optimize efficiency, we chose to use *Clk856-GAL4*, which exhibits high expression in s-LNv during early larval stages, despite also being expressed in subsets of other clock neurons (Gummadova et al., 2009). Significantly, the knockdown of Down syndrome cell adhesion molecule (Dscam1) exhibited a marked reduction in the horizontal projection distance of s-LNv axons (Figure 3-figure supplement 1A-B). To validate the role of s-LNv-expressed Dscam1 in governing axon horizontal projection, we employed the *Pdf-GAL4*, which specifically targeted s-LNvs during the larval stage. At 96 hours ALH, vertical projection showed no significant changes in *Pdf-GAL4;UAS-Dscam1-RNAi* flies, but a noticeable deficit was observed in the horizontal projection of the s-LNvs axon (Figure 3A-C). These observations strongly indicate that Dscam1 specifically regulates the horizontal projection of s-LNvs axon.

We further checked s-LNvs axon projection in several well-defined *Dscam1* mutants, including $Dscam1^{21}$, $Dscam1^{1}$, and $Dscam1^{05518}$ (Hummel et al., 2003; Schmucker et al., 2000). While all heterozygous mutants displayed normal horizontal axon projection in s-LNvs, trans-heterozygous mutants and homozygotes exhibited shortened horizontal axon projection (Figure 3D-E). Additionally, our immunostaining results indicated concentrated Dscam1 expression at the growth cone of s-LNv axons in 3rd-instar larvae (Figure 3F). Taken together, these data demonstrate that Dscam1 controls the horizontal axon projection of s-LNvs in a cell-autonomous manner.

Dscam1 is a well-recognized cell adhesion molecule that plays a crucial role in axon guidance (Chen et al., 2006; Hummel et al., 2003; Zhan et al., 2004; Zhang et al., 2019). The receptors present on growth cones sensor the extracellular axon guidance molecules to initiate the reorganization of the cellular cytoskeleton, leading to the facilitation of axonal projection. Convincingly, knockdown of the cytoskeletal molecules *tsr* (the *Drosophila* homolog of *cofilin*)

(Sudarsanam et al., 2020) and *chic* (the *Drosophila* homolog of *profilin*) (Shields et al., 2014) in s-LNvs recaptured the horizontal axon projection deficits in *Dscam1* knockdown flies or *Dscam1* mutants (Figure 3-figure supplement 1C-D). Consistently, knockdown of *Dock* and *Pak*, the guidance receptor partners of Dscam1 (Schmucker et al., 2000), or *SH3PX1*, the critical linker between Dscam1 and the cytoskeleton (Worby et al., 2001), phenocopied *Dscam1* knockdown flies or *Dscam1* mutants (Figure 3-figure supplement 1C-D). Taken together, these findings provide solid evidence to support that Dscam1 signaling as a crucial regulator of s-LNvs axon horizontal projection (Figure 3-figure supplement 1E).

Neuronal-derived Netrins act upstream of Dscam1 to govern the horizontal projection of s-LNvs axon

Two classical guidance molecules, Slit and Netrin, have been shown to specifically bind to the extracellular domain of Dscam1 (Alavi et al., 2016; Andrews et al., 2008). The *Drosophila* genome contains the sole *slit* gene and two *Netrin* genes: *Netrin-A* (*NetA*) and *Netrin-B* (*NetB*) (Harris et al., 1996; Mitchell et al., 1996). Interestingly, knockdown of both *NetA* and *NetB* (hereafter referred to as *Netrins*), rather than *slit*, resulted in the defective horizontal axon projection of s-LNvs. Convincingly, *NetA,NetB* double mutant (Brankatschk & Dickson, 2006), but not *NetA* or *NetB* single mutant, exhibited the defective horizontal axon projection of s-LNvs (Figure 4A-B and Figure 4-figure supplement 1). These results imply that two Netrin molecules function redundantly in regulating horizontal axon projection of s-LNvs.

To determine the source of Netrins, which are known to be secreted axon guidance molecules, we conducted experiments using pan-neuronal (*nsyb-GAL4*) and pan-glial (*repo-GAL4*) drivers to selectively knock down *Netrins* (Figure 4C-D). Strikingly, when *Netrins* were knocked down in neurons but not in glia, we observed severe defects in the horizontal axon projection of s-LNvs. These findings reveal that neuron-secreted Netrins serve as ligands for Dscam1, controlling the horizontal axon projection of s-LNvs.

Dorsal neuron-secreted Netrins mediate the horizontal axon projection of s-LNvs

To further identify the source of Netrins, we focused on the neurons located in the dorsolateral

209 protocerebrum, where the s-LNvs axons change their projection direction. We first excluded the
210 possibility that MB-secreted Netrins mediate the horizontal axon projection of s-LNvs, as
211 knockdown of *Netrins* with *OK107-GAL4* showed normal horizontal axon projection of s-LNvs
212 (Figure 5A-B).
213
214 The Dorsal neurons (DNs), a subset of clock neurons, also situate in the dorsolateral
215 protocerebrum. DNs are categorized into three types, DN1, DN2, and DN3 (Reinhard et al., 2022),
216 and previous studies have shown that both DN2 and DN1 form synaptic connections with s-LNvs
217 axon terminals at the adult stage (Schlichting et al., 2022). Interestingly, knockdown of *Netrins* in
218 a substantial portion of DN2, DN3, and DN1 (Kaneko et al., 1997) (*Per-GAL4,*
219 *Pdf-GAL80;UAS-Netrins-RNAi*) resulted in the defective horizontal axon projection of s-LNvs
220 (Figure 5A-B). To further validate the involvement of DNs in mediating the horizontal axon
221 projection of s-LNvs, we conducted cell ablation experiments. Notably, the impairments in the
222 horizontal axonal projection of s-LNvs due to DNs ablation were exclusively observed at 96 hours
223 ALH, which is after the occurrence of horizontal projection (Figure 5C-D). In contrast, ablating
224 crz^{+} neurons, which occupy a similar location to DNs, had no significant effects on the horizontal
225 axon projection of the s-LNvs (Figure 5-figure supplement 1). Moreover, by expressing NetB in
226 DNs in *NetA,NetB* double mutants, we successfully restored the defective horizontal axon
227 projection of s-LNvs (*$NetAB^{A}$;Per-GAL4, Pdf-GAL80;UAS-NetB)* (Figure 5E-F). These results
228 demonstrate that DNs secrete Netrins to guide the horizontal axon projection of s-LNvs.
229
230 **Newborn DNs secret Netrins to regulate the horizontal axon projection of s-LNvs**
231 Finally, we wonder which population of DNs secret Netrins to regulate the horizontal axon
232 projection of s-LNvs. Therefore, we monitored the number and location of DNs during the s-LNvs
233 axon projection and found that the number of DNs significantly increased during this process.
234 *Per-GAL4, Pdf-GAL80; UAS-mCD8::GFP* only labeled 4-5 cells at 48 hours ALH, and raise to
235 10-15 by 72 hours, and subsequently increased to approximately 25 by 96 hours ALH (Figure
236 6A-B). It is worth noting that the location of these newly formed DNs resides lateral to the
237 transition point of axon projection direction of the s-LNvs, while maintaining a basic parallelism
238 with the horizontal axon projection of the s-LNvs (Figure 6A). The sharp increase in the number

of DNs coincides remarkably with the timing of the switch in axon projection direction of the s-LNvs.

Next, we asked whether these newly generated DNs expressed Netrins. To visualize the expression of endogenous NetB, we applied the fly strains that insert either GFP or myc tag in *NetB* gene. At 72 hours ALH, we were unable to detect any NetB signals within the DNs. In contrast, at 96 hours ALH, we easily detected prominent NetB signals in approximately 6-8 newborn DNs (Figure 6C-D, Figure 6-figure supplement 1A).

Previous studies have shown that DSCAM is involved in Netrin-1-mediated axonal attraction (Andrews et al., 2008; G. Liu et al., 2009; Ly et al., 2008). In addition, DSCAM also functions as a repulsive receptor, associating with Uncoordinated-5C (UNC5C) to mediate Netrin-1-induced axon growth cone collapse (Purohit et al., 2012). To dissect the role of Netrin signaling, we ectopically expressed Netrins in neurons marked by *R78G02-GAL4* (Jenett et al., 2012; Suzuki et al., 2022), located in front of the horizontal projection of s-LNv axons, closer to the midline (Figure 6-figure supplement 1B). Expression of either NetA or NetB in *R78G02-GAL4*-labeled neurons significantly suppressed the horizontal axon projection of s-LNvs (Figure 6-figure supplement 1B-C). Taken together, these findings reveal that newborn DNs secrete Netrins to orchestrate the transition of axon projection in s-LNvs from a vertical to a horizontal direction (Figure 7).

Discussion

The mechanisms underlying axonal responses to intricate microenvironments and the precise development of axons within the brain have long remained enigmatic. In the past, researchers have identified a large number of axon guidance cues and receptors using different models *in vivo* and *in vitro* (Esther T Stoeckli, 2018). In addition, transient cell-cell interactions through intermediate targets play a crucial role in guiding axonal projection step by step towards its final destination (Chao et al., 2009; Garel & Rubenstein, 2004). The landmark midline, a crucial intermediate target, serves as a model in the majority of early studies exploring the directional transitions of axonal projections (Evans & Bashaw, 2010). However, so many neural projections do not cross the

midline that it is challenging to understand how these axon projections are guided (Goodhill, 2016). In our study, we established an excellent model to investigate the mechanism of axonal projection direction switch by the *Drosophila* s-LNvs. We discovered a coordinated growth pattern between the vertical projection of s-LNvs and the MB calyx. Furthermore, the synergistic interaction between Dscam1 expressed in s-LNvs and the emerging DN-secreted Netrins precisely modulates the transition of s-LNv axons from a vertical to a horizontal projection within a specific time window (Figure 7). These findings reveal the mechanism behind the transition of axonal projection direction, emphasizing the significance of developmental microenvironments in ensuring precise axon projection.

The dependence of s-LNv vertical projection on mushroom body calyx expansion

During our monitoring of the axonal projection of s-LNvs, we observed that the axon terminals reached the dorsolateral brain area at an early stage but continued their vertical growth. This phenomenon raises the question of what drives this growth. The mushroom body, a sophisticated central hub within the fruit fly's brain, exhibits proximity to the projection of s-LNv axons in spatial arrangement. Upon careful examination, we found a positive correlation between the vertical length increase of s-LNv axons and the growth of the mushroom body calyx (Figure 2). Remarkably, when we selectively removed KC cells, we observed a striking effect on the axonal projection of s-LNvs. The s-LNv axonal projections either stalled at the initial stage or even completely disappeared (Figure 2 and data not shown). Hence, the vertical projection of s-LNv axons is dependent on mushroom body calyx expansion. Our hypothesis is supported by the findings of Helfrich-Förster *et al.*, who reported locomotor activity and circadian rhythm defects in some MB mutants (HELFRICH-FÖRSTER et al., 2002), potentially attributed to the abnormality of s-LNvs axon. Moreover, it was observed that the MB mutants had minimal impact on the l-LNvs. This can be attributed to the fact that l-LNvs fibers emerge at a later stage during pupal development and are situated at a spatial distance from the mushroom body.

Unfortunately, we did not identify any molecules that have a discernible impact on the vertical projection of s-LNv axons through screening. This indicates that the successful completion of the vertical projection process may play a pivotal role in determining the overall existence of s-LNv

299 axonal projections. Furthermore, the dorsal projection of s-LNv axons intersects with the ventral
300 projection of neurons such as DN1 in the dorsolateral region adjacent to the calyx (Keene et al.,
301 2011), resembling the corpus callosum in mammals (Fothergill et al., 2014; Hutchins et al., 2011;
302 Keeble et al., 2006; Piper et al., 2009; Unni et al., 2012). Thus, during early developmental stages,
303 multiple guiding cues may redundantly function between the mushroom body calyx and
304 neighboring neural processes to ensure the smooth progression of neural development and
305 establish a stable brain structure. However, to gain a more comprehensive understanding, it is
306 worthwhile to explore whether the development of the mushroom body calyx influences the
307 projection of other neurons traversing the same territory and the guidance cues involved. Insights
308 from existing single-cell sequencing data obtained from multiple stages of larval life (Avalos et al.,
309 2019; Corrales et al., 2022), might offer some clues and indications.
310
311 **Netrin/Dscam signaling specifically controls the horizontal projection of s-LNv axons**
312 In this paper, when we specifically knockdown *Dscam1* in s-LNvs, we observed a significant
313 defect in the axonal horizontal projection. This suggests that Dscam1 autonomously regulates the
314 horizontal axonal projection of s-LNvs (Figure 3). Our findings align with a recent study that
315 reported abnormal horizontal axonal projection of s-LNv neurons in adult flies when Dscam1
316 mRNAs lack the long 3' UTR (Zhang et al., 2019).
317
318 The extracellular domain of Dscam1 has been verified to be capable of binding to Netrin or Slit
319 (Alavi et al., 2016). In *Drosophila*, at the midline of the embryonic central nervous system,
320 Dscam1 forms a complex with Robo1 to receive the Slit signal and promote the growth of
321 longitudinal axons (Alavi et al., 2016). In adult flies, Slit/Robo signaling restricts the medial
322 growth of s-LNv axons (Oliva et al., 2016). However, we found that reducing *Netrins* levels,
323 rather than *slit*, led to a decrease in the horizontal projection distance of s-LNv axons. Moreover,
324 in the $NetAB^{\Delta}$ double mutant, the extent of defects in the horizontal axonal projection of s-LNv
325 neurons is similar to that observed when knocking down *Dscam1* in s-LNvs. Indeed, previous
326 studies have provided evidence showcasing the widespread involvement of Dscam1 as a receptor
327 for Netrin in mediating axon growth and pathfinding (G. Liu et al., 2009; Ly et al., 2008;
328 Matthews & Grueber, 2011). When we disturbed the expression of Netrin signals in the axon

329 targeting microenvironment, it was also sufficient to cause abnormal s-LNv projection (Figure
330 6-figure supplement 1B-C). Therefore, our findings suggest that Netrin, as a ligand for Dscam1,
331 regulates the process of switching axon projection direction (Figure 4).
332
333 **The newborn DNs-secreted Netrin coordinates with s-LNv-expressed Dscam1 to switch the**
334 **projection direction of s-LNv axons**
335 While the midline serves as a prominent landmark, it presents a daunting challenge to comprehend
336 the guidance and directional transitions of axons in many neural projections that do not actually
337 cross this central axis (Evans & Bashaw, 2010). Following vertical projection, the s-LNvs growth
338 cones remain within the dorsolateral area for at least 48 hours before initiating horizontal
339 projection (Figure 1). This phenomenon aligns harmoniously with the outcomes observed in
340 earlier studies that the axonal growth of other types of neurons slows down at the specific choice
341 point, the midline (Bak & Fraser, 2003; Godement et al., 1994; T. Li et al., 2021), indicating that
342 the dorsolateral area serves as an intermediate targets to facilitate the subsequent phase of s-LNvs
343 projection journey.
344
345 Extracellular cues released by the final or intermediate targets play a crucial role in guiding axonal
346 projection. The axon terminals of s-LNvs showed close spatial associations with the somas and
347 processes of DNs. In this study, the knockdown of *Netrins* specifically in per^{+},Pdf^{-} neurons, but
348 not in the mushroom body, resulted in axon projection defects in s-LNvs (Figure 5). Furthermore,
349 the ablation of DNs resulted in the inhibition of horizontal growth of s-LNvs axons (Figure 5).
350 These findings suggest that the Netrin signaling microenvironment secreted by DNs is involved in
351 regulating the horizontal projection of s-LNv axons.
352
353 **Ideas and Speculation**
354 The emergence of NetB-positive DNs and the aberrant axonal projection of s-LNv neurons caused
355 by DN ablation occur concurrently during development (Figure 6). In *Drosophila*, three types of
356 circadian oscillator neurons, including two DN1s, two DN2s, and 4-5 s-LNvs, can be identified as
357 early as embryonic stage 16 (Houl et al., 2008). The DN3 group, which represents the largest
358 contingent within the central circadian neuron network with over 35 neurons, emerges during the

larval stage (T. Liu et al., 2015). Little is known about the function of DN3 neurons, particularly during the larval stage. Due to the lack of cell-specific labeling tools, we can only speculate about the identity of these newly generated Netrin-secreting neurons as DN3s based on their spatial distribution. Taken together, these results unveil a novel regulatory mechanism where axons, during the process of pathfinding, await guidance cues from newly born guidepost cells. This enables a switch in the direction of axon projection, facilitating the axon's subsequent journey.

Acknowledgements

We thank Dr. Haihuai He for providing *Dscam1* mutant flies; Dr. Yufeng Pan for the fly line used in cell ablation; Dr. Renjun Tu for the *NetB-GFP* fly; Dr. Xuan Guo for collecting the tool flies; the Bloomington stock center and Tsinghua fly center for providing flies; Dr. Tzumin Lee for Dscam1 antibodies; Dr. Ranhui Duan HA-NetA and HA-NetB plasmids. This work was supported by the National Natural Science Foundation of China (32170970 to Y.T., 32230039 to J.H.), STI 2030- Major Projects-2021ZD0202500 to J.H., and the Guangdong Key Project-2018B030335001 to J.H.

Author Contributions

J. L. designed and performed experiments, interpreted data and wrote the manuscript; Y. W. performed experiments, Y.T. designed experiments, interpreted data and wrote the manuscript; J. H. designed experiments, interpreted data, wrote the manuscript, and supervised the project.

Declaration of Interests

The authors declare no competing financial interests.

Corresponding authors

Correspondence to: Yao Tian and Junhai Han, School of Life Science and Technology, Southeast University, 2 Sipailou Road, Nanjing 210096, China. Tel: +86-25-83790962; Fax: +86-25-83790962; E-mail: yaotian@seu.edu.cn, junhaihan@seu.edu.cn.

Figure legends

Figure 1. s-LNvs axon projection dynamics during the larval stage.

(A) Images showing the growth process of s-LNvs during larval development. Larval brains were stained with anti-PDF (white) and HRP (magenta) antibodies. Different time points indicate the hours after larval hatching (ALH).

(B) Left panel: schematic diagram illustrating the method used to measure the degree of vertical projection. One hemisphere of the larvae brain is depicted. larval neuropil (gray), s-LNvs (green), optic lobe (blue). Right panel: graphs showing the average vertical projection length at different developmental stages, presented as mean ± SD.

(C) Left panel: schematic diagram illustrating the method used to measure the degree of horizontal projection. Right panel: graphs showing the average horizontal projection (A.U.: arbitrary unit) at different developmental stages, presented as mean ± SD. The red line segment indicates the stage at which the axonal projection undergoes a directional transition.

(D) Schematic representation of s-LNvs vertical to horizontal projection directional shift during 72 -96 hours ALH. One hemisphere of the larvae brain (gray), larval neuropil (white), s-LNvs (green).

For (B), (C), 8 h (n = 7), 24 h (n = 10), 48 h (n = 14), 72 h (n = 16), 96 h (n = 13), 120 h (n = 16).

Figure 2. Development of vertical projection process alongside Mushroom Body growth.

(A) Top: Spatial position relationship between calyx and s-LNvs labeled by *OK107-GAL4*, which labels MB γ and α'β' neurons, at different developmental time points. Bottom: Spatial position relationship between calyx and s-LNvs labeled by *Tab2-201Y-GAL4*, which labels MB γ neurons, Larvae brains were stained with anti-PDF (green) and GFP (magenta) antibodies. Different time indicated hours ALH. The white dotted line indicates the calyx region.

(B) Graphs showing the mushroom body calyx's area and vertical projection length averaged over different development stage are presented as mean ± SD. *OK107*: 24 h (n = 10), 48 h (n = 8), 72 h (n = 12), 96 h (n = 12), 120 h (n = 9). Pearson's r = 0.9987, P < 0.0001. *Tab2-201Y*: 24 h (n = 6), 48 h (n = 12), 72 h (n = 13), 96 h (n = 13), 120 h (n = 11). Pearson's r = 0.9963, P = 0.0003.

(C) Schematic representation of synergetic development of s-LNvs vertical projection and mushroom body calyx. Mushroom body (purple), s-LNvs (Green).

(D) Images of mushroom body ablation in the developing larval stages. Larvae brains were stained

with anti-PDF (white) and HRP (magenta) antibodies. Different time indicated hours ALH.

(E) Quantification of vertical projection length in Control *(Tab2-201Y >GFP*) and Ablation (*Tab2-201Y >GFP,rpr,hid*) flies. Data are presented as mean ± SD. Control: 24 h (n = 6), 48 h (n = 14), 72 h (n = 13), Ablation: 24 h (n = 6), 48 h (n = 12), 72 h (n = 12). Two-tailed Student's t tests were used. ns, $p > 0.05$; ****$p < 0.0001$.

Figure 2- figure supplement 1. Validation of MB ablation efficiency.

(A) Images of mushroom body ablation in the developing larval stages. Larvae brains were stained with anti-GFP (green) and HRP (magenta) antibodies. Different time indicated after larval hatching (ALH).

(B) Quantification of MB calyx area in Control *(201Y >GFP*) and Ablation (*201Y >GFP,rpr,hid*) flies. Data are presented as mean ± SD. Control: 24 h (n = 6), 48 h (n = 12), 72 h (n = 13), Ablation: 24 h (n = 6), 48 h (n = 12), 72 h (n = 12). Two-tailed Student's t tests, ****$p < 0.0001$.

Figure 3. Critical role of Dscam1 in horizontal projection.

(A) Images of s-LNvs in *Pdf >GFP* and *Pdf >GFP, Dscam1^{RNAi}* fly. White line segment represents the horizontal projection distance of s-LNvs. Larvae brains were stained with anti-PDF (white) and HRP (magenta) antibodies at 96 hours ALH. *Pdf >GFP*: (n = 13), *Pdf >GFP, Dscam1^{RNAi}*: (n = 15).

(B) Quantification of vertical projection length in *Pdf >GFP* and *Pdf >GFP, Dscam1^{RNAi}* flies. Data are presented as mean ± SD. Two-tailed Student's t tests, ns, $p > 0.05$.

(C) Quantification of horizontal A.U. in *Pdf >GFP* and *Pdf >GFP, Dscam1^{RNAi}* flies. Data are presented as mean ± SD. Two-tailed Student's t tests, ****$p < 0.0001$.

(D) Images of *Dscam1* mutant s-LNvs projection phenotype. Larvae brains were collected at late 3rd larvae. Heads were stained with anti-PDF (white) and HRP (magenta) antibodies.

(E) Quantification of horizontal A.U. in *Dscam1* mutant flies. Data are presented as mean ± SD. w^{1118} (n = 22) *Dscam1^{21}*/+ (n = 5), *Dscam1^{1}*/+ (n = 8), *Dscam1^{05518}*/+ (n = 10), *Dscam1^{21}/Dscam1^{05518}* (n = 6), *Dscam1^{21}/Dscam1^{1}* (n = 10), *Dscam1^{05518}* (n = 14). One-way ANOVA with Tukey's post hoc, ns, $p > 0.05$, ****$p < 0.0001$.

(F) Endogenous Dscam1 co-localizes with the s-LNvs axon terminal. *Pdf >GFP* fly heads were

449 collected at 120 h ALH and stained with anti-Dscam1 (red). The white dotted line indicates the
450 s-LNvs axon.
451
452 **Figure 3- figure supplement 1. Dscam1 and its downstream signaling pathway in s-LNvs**
453 **horizontal projection.**
454 (A) Images of immunostained in *Clk856-GAL4* knockdown Dscam1. Larvae brains were collected
455 at late 3rd larvae. Heads were stained with anti-PDF (white) and HRP (magenta) antibodies.
456 (B) Quantification of horizontal A.U. in *Clk856-GAL4* knockdown Dscam1. Data are presented as
457 mean ± SD. *Clk856-GAL4/+* (n = 6), *Clk856-GAL4 >Dscam1*^{RNAi} (n = 10). Two-tailed Student's t
458 tests, ****p < 0.0001.
459 (C) Images of immunostained in *Pdf-GAL4* knockdown cytoskeleton-associated regulatory
460 proteins and Dscam1 interaction molecule. Larvae brains were collected at late 3rd larvae. Heads
461 were stained with anti-PDF (white) and HRP (magenta) antibodies.
462 (D) Quantification of horizontal A.U. in *Pdf-GAL4* knockdown *Dscam1* interaction molecule and
463 cytoskeleton-associated regulatory proteins. Data are presented as mean ± SD. *Pdf-GAL4/+* (n =
464 14), *Pdf-GAL4 >tsr*^{RNAi} (n = 6), *Pdf-GAL4 >chic*^{RNAi} (n = 8), *Pdf-GAL4 >SH3PX1*^{RNAi} (n = 6),
465 *Pdf-GAL4 >Dock*^{RNAi} (n = 7), *Pdf-GAL4 >pak*^{RNAi} (n = 6). One-way ANOVA with Dunnett's post
466 hoc, ***p < 0.001 , ****p < 0.0001.
467 (E) Schematic representation of Dscam1 mediates s-LNvs horizontal projection downstream
468 signaling pathways. Dscam1 (brown) activates the downstream signaling cascade involving Dock
469 (cyan), SH3PX1 (yellow), Pak (blue), and cofilin/profilin (depicted in purple and blue balls,
470 respectively). These signaling events induce alterations in cell cytoskeleton proteins (gray balls),
471 facilitating the guidance of horizontal projection
472
473 **Figure 4. Neuron-derived Netrin guides s-LNvs horizontal projection.**
474 (A) Images of immunostained in w^{1118}, $NetA^{\Delta}$, $NetB^{\Delta}$ and $NetAB^{\Delta}$ fly. Larvae brains were collected
475 at late 3rd larvae. Heads were stained with anti-PDF (white) and HRP (magenta) antibodies.
476 (B) Quantification of horizontal A.U. w^{1118}, $NetA^{\Delta}$, $NetB^{\Delta}$ and $NetAB^{\Delta}$ fly. Data are presented as
477 mean ± SD, w^{1118} (n = 17), $NetA^{\Delta}$ (n = 15), $NetB^{\Delta}$ (n = 24), $NetAB^{\Delta}$ (n = 23). One-way ANOVA

with Dunnett's post hoc, ns, $p > 0.05$, ***$p < 0.001$.

(C) Images of immunostained in *nSyb-GAL4* and *repo-GAL4* knockdown *Netrins*. Larvae brains were collected at late 3rd larvae heads were stained with anti-PDF (white) and HRP (magenta) antibodies.

(D) Quantification of horizontal A.U. in *nSyb-GAL4* and *repo-GAL4* knockdown *Netrins* fly. Data are presented as mean ± SD. *nSyb-GAL4/+* (n = 13), *nSyb-GAL4 >Netrins^{RNAi}* (n = 16), *repo-GAL4/+* (n = 34), *repo-GAL4 >Netrins^{RNAi}* (n = 20). Two-tailed Student's t tests, ns, $p > 0.05$, ***$p < 0.001$.

Figure 4- figure supplement 1. Identifying the upstream signal of Dscam1.

(A) Images of immunostained in *tubulin-GAL4/+*, *tubulin-GAL4 >Netrins^{RNAi}*, *tubulin-GAL4 >slit^{RNAi}* fly. Larvae brains were heads were collected at late 3rd larvae. Head stained with anti-PDF (white) and HRP (magenta) antibodies.

(B) Quantification of horizontal A.U. in *tubulin-GAL4/+, tubulin-GAL4 >Netrins^{RNAi,} tubulin-GAL4 >slit^{RNAi}* fly. Data are presented as mean ± SD. *tubulin-GAL4/+* (n = 13), *tubulin-GAL4 >Netrins^{RNAi}* (n = 20), *tubulin-GAL4 >slit^{RNAi}* (n = 9). One-way ANOVA with Dunnett's post hoc, ns, $p > 0.05$, **$p < 0.01$.

Figure 5. Netrin secreted by DN neurons guides time-specific horizontal projection of s-LNvs.

(A) Images of immunostained in *OK107-GAL4* and *per-GAL4, Pdf-GAL80* knockdown *Netrins.* Larvae brains were collected at late 3rd larvae. Heads were stained with anti-PDF (white) and HRP (magenta) antibodies.

(B) Quantification of horizontal A.U. in *OK107-GAL4* and *per-GAL4, Pdf-GAL80* knockdown *Netrins* fly. Data are presented as mean ± SD. *OK107-GAL4/+* (n = 20), *OK107-GAL4 >Netrins^{RNAi}* (n = 13). *per-GAL4, Pdf-GAL80/+* (n = 18), *per-GAL4, Pdf-GAL80 >Netrins^{RNAi}* (n = 16), Two-tailed Student's t tests for *OK107-GAL4* knockdown *Netrins*, ns, $p > 0.05$. Mann-Whitney test for *per-GAL4, Pdf-GAL80* knockdown *Netrins*, ****$p < 0.0001$.

(C) Images of DN ablation in the developing larval stages. Larvae brains were stained with

anti-PDF (white) and HRP (magenta) antibodies. Different time indicated hours ALH.

(D) Quantification of horizontal A.U. in Control (*per-GAL4, Pdf-GAL80 >GFP*) and Ablation (*per-GAL4, Pdf-GAL80 >GFP,rpr,hid*) flies. Data are presented as mean ± SD. Control: 72 h (n = 5), 96 h (n = 12), Ablation: 72 h (n = 5), 96 h (n = 10). Two-tailed Student's t tests were used to compare conditions. ns, $p > 0.05$, ****$p < 0.0001$.

(E) Images of immunostained in *per-GAL4, Pdf-GAL80* overexpress *NetB* in $NetAB^{\Delta}$. Larvae brains were collected at late 3rd larvae. Heads were stained with anti-PDF (white) and HRP (magenta) antibodies.

(F) Quantification of horizontal A.U. in *per-GAL4, Pdf-GAL80* overexpress *NetB* in $NetAB^{\Delta}$. Data are presented as mean ± SD. $NetAB^{\Delta}$*, UAS-NetB* (n = 12), $NetAB^{\Delta}$*, per-GAL4,Pdf-GAL80 /+* (n = 5), $NetAB^{\Delta}$*,per-GAL4,Pdf-GAL80 >UAS-NetB* (n = 9). One-way ANOVA with Bonferroni post hoc, ns, $p > 0.05$, ***$p < 0.001$.

Figure 5- figure supplement 1. Ablation of DN neurons leads to reduced s-LNvs horizontal projection.

(A) Images of per-GAL4, pdf-GAL80 and crz-GAL4 ablation. Larvae brains were stained with anti-PDF(white) and HRP(magenta) antibodies at 120 h ALH.

(B) Quantification of horizontal A.U. in *per-GAL4, Pdf-GAL80* and *crz-GAL4* ablation fly. Data are presented as mean ± SD. *per-GAL4, Pdf-GAL80 >GFP* (n = 14), *per-GAL4, Pdf-GAL80 >GFP,rpr,hid* (n = 20), *crz-GAL4 >GFP* (n = 4), *crz-GAL4 >GFP,rpr,hid* (n = 3). Two-tailed Student's t tests, ns, $p > 0.05$; ****$p < 0.0001$.

Figure 6. Dynamic changes in DN neurons coordinated with s-LNvs axonal targeting.

(A) Top: Images of s-LNvs axon and DNs growth process in the developing larval stages. Larvae brains were stained with anti-PDF (white) and GFP (green) antibodies. Different time indicated hours ALH are shown. Bottom: schematic diagram of s-LNvs horizontal projection and the corresponding increase in the number of DN neurons. s-LNvs axon (gray), DN neurons (green).

(B) Quantification of the number of DN neurons labeled by *per-GAL4, Pdf-GAL80* at different developmental stages. Data are presented as mean ± SD.

(C) Images of newborn DN neurons were colocalized with *Netrin-B* at different developmental

538 times. Larvae brains were stained with anti-GFP (green), mcherry (red) and PDF (white)
539 antibodies. Different time indicated hours ALH. The white arrow demarcates the co-localization of
540 red and green signals.
541 (D) Schematic representation s-LNvs projection directional transition and the corresponding
542 increase in the number of DN neurons. s-LNvs axon (gray), DN neurons (green), newborn DN
543 neurons (light green at 72 h, orange at 96 h).
544
545 **Figure 6- figure supplement 1. Anterior Netrin ectopic expression reduces horizontal**
546 **projection length.**
547 (A) Left: Schematic representation s-LNvs projection directional transition and the corresponding
548 increase in the number of DN neurons. s-LNvs axon (gray), DN neurons(green), newborn DN
549 neurons (light green at 72 h, orange at 96h). Right: images of DN neurons were colocalized with
550 Netrin-B at different developmental times. Larvae brains were stained with anti-Myc (red) and
551 GFP (green) antibodies. Different time indicated after larval hatching (ALH). The white arrow
552 demarcates the co-localization of red and green signals.
553 (B) Images of Netrin ectopic expressed in *R78G02-GAL4*. Larvae brains were collected at late 3rd
554 larvae. Heads were stained with anti-PDF (white) and HRP (magenta) antibodies.
555 (C) Quantification of horizontal A.U. in Netrin ectopic expressed in *R78G02-GAL4* fly. Data are
556 presented as mean ± SD. *R78G0-GAL4/+* (n = 11), *R78G02-GAL4 >UAS-NetA*^{OE} (n = 6),
557 *R78G02-GAL4 >UAS-NetB*^{OE} (n = 11). One-way ANOVA with Dunnett's post hoc, ***p < 0.001,
558 ****p < 0.0001.
559
560 **Figure 7. Dynamic cellular molecular environment during the s-LNv projection directional**
561 **shift.**
562 Cartoon depicting the dynamic cellular molecular microenvironment during the axonal projection
563 directional shift from vertical to horizontal projection in s-LNvs. 72 h and 96 h represent 72 h and
564 96 h after larval hatching, respectively. s-LNvs (blue), neuropile (pink), brain lobe (gray circule),
565 DNs (orange and light orange circles), optic lobe (gray dotted line), Netrin (Orange combination
566 molding), Dscam1 (pruple).
567

Materials and methods

Fly Genetics

The flies were maintained on standard medium at 25°C with 60–80% relative humidity. The wild-type flies used in this study were w^{1118}. The *Dscam1 (CG17800)* null mutant allele, $Dscam1^{21}$, was obtained from Haihuai He's laboratory. *UAS-rprC;;UAS-hid* fly were kindly provided by Yufeng Pan's laboratory. The RNAi lines used in these studies were purchased from Tsinghua University; other flies were obtained from Bloomington Stock Center. Full genotypes of the flies shown in the main figures and supplemental figures are listed in Supplementary File 2.

Generation of Transgenic Flies

To generate the NetA and NetB transgenes, the full-length NetA cDNAs and the the full-length NetB cDNAs were sub-cloned into the pUAST vectors and injected into w^{1118} flies.

Antibodies

Antibodies were obtained from Developmental Studies Hybridoma Bank (anti-PDF, anti-FasII) Jackson Immuno Research (anti-HRP), Invitrogen (anti-GFP Alexa-488 goat anti-chicken IgY), Rockland (anti-RFP), and Abcam (Alexa-555 goat anti-rabbit IgG, Alexa-647 goat anti-mouse IgG, Alexa 488 goat anti-rabbit IgG and Alexa 488 goat anti-mouse IgG), gifted from Tzumin Lee's Lab (anti-Dscam1).

Collection larvae

~100 females lay eggs on the collecting medium (1% agar and 30% juice) in Petri dishes for a 4-hour period. To obtain larvae of defined ages, freshly emerged larvae were selected at 2 hours' intervals. They were then allowed to grow on the cornmeal medium until they reached the desired age, and they were dissected at 0.5 hour intervals.

Immunostaining

Larvae brain were dissected in phosphate-buffered saline (PBS) and fixed with 4% formaldehyde (PFA) for 25 min at room temperature. After fixation and three washes with 0.3% Triton X-100 in PBS. Brains were blocked with 5% goat serum in PBS with 0.3% Triton X-100 at 4°C 1 hour and

598 were incubated with primary antibodies in PBS with 0.3% Triton X-100 at 4°C overnight. After
599 four washes, brains were incubated with secondary antibodies in PBS with 0.3% Triton X-100 at
600 room temperature for 2-3 h. After four washes, brains were mounted for microscopy in vectashield
601 without DAPI (Vector Laboratories). Primary antibodies were mouse anti-PDF (1:300), mouse
602 anti-FasII (1:50), Rabbit anti- HRP (1:500), mouse anti-Dscam1- 18mAb (1:20), rabbit anti-GFP
603 (1:200), rabbit anti-RFP (1:500), chicken anti-GFP (1:2000), rabbit anti-Myc (1:200), Secondary
604 antibodies were Alexa Fluor 555 goat anti-Rabbit IgG (1:200), Alexa Fluor 647 goat anti-mouse
605 IgG (1:200), Alexa Fluor 488 goat anti-rabbit IgG (1:200) and Alexa Fluor 488 goat anti-chicken
606 IgY (1:200). Samples were imaged on an LSM 700 confocal microscope (Zeiss).
607
608 ImageJ software (National Institutes of Health) was used for the quantification vertical and
609 horizontal axonal length of PDF immunostaining in s-LNvs. For s-LNvs horizontal measurements,
610 results are presented as A.U. representing the fraction between the lengths of the horizontal
611 projections divided by the distance between cell bodies and midline. Data are presented as means
612 ± standard deviation from examined brains.
613
614 RNAi Screening
615 The UAS-RNAi line were obtained from Tsinghua Fly Center, and Bloomington Drosophila Stock
616 Center. The RNAi screen fly was generated as follows: recombine *Pdf-GAL4* with
617 *UAS-mCD8-GFP* or use *Clk856-GAL4* directly, which has a broader expression pattern.
618 UAS-RNAi males were crossed to this two screening lines, and the resulting flies were kept at
619 25 °C, and dissected at desired age.
620
621 Neuron ablation
622 *Tab2-201Y-GAL4* which is expressed in larval mushroom body γ neuron and
623 *per-GAL4,Pdf-GAL80* which is expressed in DN neurons was used to drive the expression of
624 reaper (rpr) and hid .The GAL4 flies integrated UAS-GFP, and the efficiency of ablation was
625 confirmed by GFP signals in mushroom body and DN neurons. Animals were raised at 25°C to
626 desired time.
627

628 Quantification and Statistical Analysis

629 Statistical analysis was performed with GraphPad Prism V8.0.2 software. Data are presented as
630 means ± standard deviation (SD). Shapiro-Wilk test was used to verify whether the data
631 conformed to the normal distribution. F test was used to verify homogenous variances between
632 two groups. Bartlett test was used to verify homogenous variances three or more conditions and
633 genotypes. Statistical significance was set as: * $p < 0.05$, ** $p < 0.01$, *** $p < 0.001$; **** $p <$
634 0.0001, ns, no significance, $p > 0.05$. Statistical details of the experiments are found in the figure
635 legends.

636

637

638 **Supplemental Information**

639 Supplementary File 1. Key resource table

640 Supplementary File 2. Full genotypes of the flies that are shown in the main figures, supplemental
641 figures.

642 Supplementary File 3. List of genes used for RNAi screen

643

644 **Reference**

645 Agrawal, P., & Hardin, P. E. (2016). The drosophila receptor protein tyrosine phosphatase LAR is
646 required for development of circadian pacemaker neuron processes that support rhythmic activity
647 in constant darkness but not during light/dark cycles. *Journal of Neuroscience*, *36*(13), 3860–
648 3870. https://doi.org/10.1523/JNEUROSCI.4523-15.2016

649 Alavi, M., Song, M., King, G. L. A., Gillis, T., Propst, R., Lamanuzzi, M., Bousum, A., Miller, A.,
650 Allen, R., & Kidd, T. (2016). Dscam1 Forms a Complex with Robo1 and the N-Terminal
651 Fragment of Slit to Promote the Growth of Longitudinal Axons. *PLoS Biology*, *14*(9), 1–31.
652 https://doi.org/10.1371/journal.pbio.1002560

653 Andrews, G. L., Tanglao, S., Farmer, W. T., Morin, S., Brotman, S., Berberoglu, M. A., Price, H.,
654 Fernandez, G. C., Mastick, G. S., Charron, F., & Kidd, T. (2008). Dscam guides embryonic
655 axons by Netrin-dependent and -independent functions. *Development*, *135*(23), 3839–3848.
656 https://doi.org/10.1242/dev.023739

657 Araújo, S. J., & Tear, G. (2003). Axon guidance mechanisms and molecules: Lessons from
658 invertebrates. *Nature Reviews Neuroscience*, *4*(11), 910–922. https://doi.org/10.1038/nrn1243

659 Avalos, C. B., Brugmann, R., & Sprecher, S. G. (2019). Single cell transcriptome atlas of the
660 drosophila larval brain. *ELife*, *8*, 1–25. https://doi.org/10.7554/eLife.50354

661 Bak, M., & Fraser, S. E. (2003). Axon fasciculation and differences in midline kinetics between
662 pioneer and follower axons within commissural fascicles. *Development*, *130*(20), 4999–5008.
663 https://doi.org/10.1242/dev.00713

664 Brankatschk, M., & Dickson, B. J. (2006). Netrins guide Drosophila commissural axons at short range.
665 *Nature Neuroscience*, *9*(2), 188–194. https://doi.org/10.1038/nn1625

666 Bron, R., Vermeren, M., Kokot, N., Andrews, W., Little, G. E., Mitchell, K. J., & Cohen, J. (2007).
667 Boundary cap cells constrain spinal motor neuron somal migration at motor exit points by a
668 semaphorin-plexin mechanism. *Neural Development*, *2*, 21.
669 https://doi.org/10.1186/1749-8104-2-21

670 Cang, J., & Feldheim, D. A. (2013). Developmental mechanisms of topographic map formation and
671 alignment. *Annual Review of Neuroscience*, *36*, 51–77.
672 https://doi.org/10.1146/annurev-neuro-062012-170341

673 Chan, C. E., & Odde, D. J. (2008). Traction dynamics of filopodia on compliant substrates. *Science*

674 *(New York, N.Y.)*, *322*(5908), 1687–1691. https://doi.org/10.1126/science.1163595

675 Chao, D. L., Ma, L., & Shen, K. (2009). Transient cell-cell interactions in neural circuit formation.
676 *Nature Reviews Neuroscience*, *10*(4), 262–271. https://doi.org/10.1038/nrn2594

677 Chédotal, A., Richards, L. J., Dent, E. W., Gupton, S. L., Frank, B., Adams, R. H., Eichmann, A.,
678 Engle, E. C., Raper, J., & Mason, C. (2012). *Navigating Intermediate Targets : The Nervous*
679 *System Midline Navigating Intermediate Targets : The Nervous System Midline*.
680 https://doi.org/10.1101/cshperspect.a002055

681 Chen, B. E., Kondo, M., Garnier, A., Watson, F. L., Püettmann-Holgado, R., Lamar, D. R., &
682 Schmucker, D. (2006). The Molecular Diversity of Dscam Is Functionally Required for Neuronal
683 Wiring Specificity in Drosophila. *Cell*, *125*(3), 607–620.
684 https://doi.org/10.1016/j.cell.2006.03.034

685 Corrales, M., Cocanougher, B. T., Kohn, A. B., Wittenbach, J. D., Long, X. S., Lemire, A., Cardona,
686 A., Singer, R. H., Moroz, L. L., & Zlatic, M. (2022). A single-cell transcriptomic atlas of
687 complete insect nervous systems across multiple life stages. *Neural Development*, *17*(1), 8.
688 https://doi.org/10.1186/s13064-022-00164-6

689 Cyran, S. A., Yiannoulos, G., Buchsbaum, A. M., Saez, L., Young, M. W., & Blau, J. (2005). The
690 double-time protein kinase regulates the subcellular localization of the Drosophila clock protein
691 period. *The Journal of Neuroscience : The Official Journal of the Society for Neuroscience*,
692 *25*(22), 5430–5437. https://doi.org/10.1523/JNEUROSCI.0263-05.2005

693 de Ramon Francàs, G., Zuñiga, N. R., & Stoeckli, E. T. (2017). The spinal cord shows the way – How
694 axons navigate intermediate targets. *Developmental Biology*, *432*(1), 43–52.
695 https://doi.org/10.1016/j.ydbio.2016.12.002

696 Derijck, A. A. H. A., Van Erp, S., & Pasterkamp, R. J. (2010). Semaphorin signaling: molecular
697 switches at the midline. *Trends in Cell Biology*, *20*(9), 568–576.
698 https://doi.org/10.1016/j.tcb.2010.06.007

699 Dickson, B. J. (2002). Molecular mechanisms of axon guidance. *Science (New York, N.Y.)*, *298*(5600),
700 1959–1964. https://doi.org/10.1126/science.1072165

701 Evans, T. A., & Bashaw, G. J. (2010). *Axon guidance at the midline : of mice and flies*. 79–85.
702 https://doi.org/10.1016/j.conb.2009.12.006

703 Fothergill, T., Donahoo, A.-L. S., Douglass, A., Zalucki, O., Yuan, J., Shu, T., Goodhill, G. J., &

Richards, L. J. (2014). Netrin-DCC Signaling Regulates Corpus Callosum Formation Through Attraction of Pioneering Axons and by Modulating Slit2-Mediated Repulsion. *Cerebral Cortex*, *24*(5), 1138–1151. https://doi.org/10.1093/cercor/bhs395

Garel, S., & López-Bendito, G. (2014). Inputs from the thalamocortical system on axon pathfinding mechanisms. *Current Opinion in Neurobiology*, *27*, 143–150. https://doi.org/https://doi.org/10.1016/j.conb.2014.03.013

Garel, S., & Rubenstein, J. L. R. (2004). Intermediate targets in formation of topographic projections: Inputs from the thalamocortical system. *Trends in Neurosciences*, *27*(9), 533–539. https://doi.org/10.1016/j.tins.2004.06.014

Gezelius, H., & López-Bendito, G. (2017). Thalamic neuronal specification and early circuit formation. *Developmental Neurobiology*, *77*(7), 830–843. https://doi.org/https://doi.org/10.1002/dneu.22460

Godement, P., Wang, L. C., & Mason, C. A. (1994). Retinal axon divergence in the optic chiasm: dynamics of growth cone behavior at the midline [published erratum appears in J Neurosci 1995 Mar;15(3):following table of contents]. *The Journal of Neuroscience*, *14*(11), 7024 LP – 7039. https://doi.org/10.1523/JNEUROSCI.14-11-07024.1994

Goodhill, G. J. (2016). Can Molecular Gradients Wire the Brain? *Trends in Neurosciences*, *39*(4), 202–211. https://doi.org/10.1016/j.tins.2016.01.009

Gorla, M., & Bashaw, G. J. (2020). Molecular mechanisms regulating axon responsiveness at the midline. *Developmental Biology*, *466*(1), 12–21. https://doi.org/https://doi.org/10.1016/j.ydbio.2020.08.006

Gummadova, J. O., Coutts, G. A., & Glossop, N. R. J. (2009). Analysis of the drosophila clock promoter reveals heterogeneity in expression between subgroups of central oscillator cells and identifies a novel enhancer region. *Journal of Biological Rhythms*, *24*(5), 353–367. https://doi.org/10.1177/0748730409343890

Hardin, P. E. (2017). VRILLE Controls PDF Neuropeptide Accumulation and Arborization Rhythms in Small Ventrolateral Neurons to Drive Rhythmic Behavior in Drosophila VRILLE Controls PDF Neuropeptide Accumulation and Arborization Rhythms in Small Ventrolateral Neurons to Drive R. *Current Biology*, *27*(22), 3442-3453.e4. https://doi.org/10.1016/j.cub.2017.10.010

Harris, R., Sabatelli, L. M., & Seeger, M. A. (1996). Guidance cues at the Drosophila CNS midline: identification and characterization of two Drosophila Netrin/UNC-6 homologs. *Neuron*, *17*(2),

217–228. https://doi.org/10.1016/s0896-6273(00)80154-3

Helfrich-Förster, C. (1997). Development of pigment-dispersing hormone-immunoreactive neurons in the nervous system of Drosophila melanogaster. *Journal of Comparative Neurology*, *380*(3), 335–354. https://doi.org/10.1002/(SICI)1096-9861(19970414)380:3<335::AID-CNE4>3.3.CO;2-M

Helfrich-Förster, C., Shafer, O. T., Wülbeck, C., Grieshaber, E., Rieger, D., & Taghert, P. (2007). Development and morphology of the clock-gene-expressing lateral neurons of Drosophila melanogaster. *The Journal of Comparative Neurology*, *500*(1), 47–70. https://doi.org/10.1002/cne.21146

HELFRICH-FÖRSTER, C., WULF, J., & DE BELLE, J. S. (2002). MUSHROOM BODY INFLUENCE ON LOCOMOTOR ACTIVITY AND CIRCADIAN RHYTHMS IN DROSOPHILA MELANOGASTER. *Journal of Neurogenetics*, *16*(2), 73–109. https://doi.org/10.1080/01677060213158

Houl, J. H., Ng, F., Taylor, P., & Hardin, P. E. (2008). CLOCK expression identifies developing circadian oscillator neurons in the brains of Drosophila embryos. *BMC Neuroscience*, *9*, 119. https://doi.org/10.1186/1471-2202-9-119

Hummel, T., Vasconcelos, M. L., Clemens, J. C., Fishilevich, Y., Vosshall, L. B., & Zipursky, S. L. (2003). Axonal targeting of olfactory receptor neurons in Drosophila is controlled by Dscam. *Neuron*, *37*(2), 221–231. https://doi.org/10.1016/S0896-6273(02)01183-2

Hutchins, B. I., Li, L., & Kalil, K. (2011). Wnt/calcium signaling mediates axon growth and guidance in the developing corpus callosum. *Developmental Neurobiology*, *71*(4), 269–283. https://doi.org/https://doi.org/10.1002/dneu.20846

Jenett, A., Rubin, G. M., Ngo, T.-T. B., Shepherd, D., Murphy, C., Dionne, H., Pfeiffer, B. D., Cavallaro, A., Hall, D., Jeter, J., Iyer, N., Fetter, D., Hausenfluck, J. H., Peng, H., Trautman, E. T., Svirskas, R. R., Myers, E. W., Iwinski, Z. R., Aso, Y., … Zugates, C. T. (2012). A GAL4-driver line resource for Drosophila neurobiology. *Cell Reports*, *2*(4), 991–1001. https://doi.org/10.1016/j.celrep.2012.09.011

Kaas, J. H. (1997). Topographic maps are fundamental to sensory processing. *Brain Research Bulletin*, *44*(2), 107–112. https://doi.org/10.1016/s0361-9230(97)00094-4

Kahn, O. I., & Baas, P. W. (2016). Microtubules and Growth Cones: Motors Drive the Turn. *Trends in*

764 *Neurosciences*, *39*(7), 433–440. https://doi.org/https://doi.org/10.1016/j.tins.2016.04.009

765 Kaneko, M., Helfrich-Förster, C., & Hall, J. C. (1997). Spatial and temporal expression of the period

766 and timeless genes in the developing nervous system of drosophila: Newly identified pacemaker

767 candidates and novel features of clock gene product cycling. *Journal of Neuroscience*, *17*(17),

768 6745–6760. https://doi.org/10.1523/jneurosci.17-17-06745.1997

769 Keeble, T. R., Halford, M. M., Seaman, C., Kee, N., Macheda, M., Anderson, R. B., Stacker, S. A., &

770 Cooper, H. M. (2006). The Wnt Receptor Ryk Is Required for Wnt5a-Mediated Axon Guidance

771 on the Contralateral Side of the Corpus Callosum. *The Journal of Neuroscience*, *26*(21), 5840 LP

772 – 5848. https://doi.org/10.1523/JNEUROSCI.1175-06.2006

773 Keene, A. C., Mazzoni, E. O., Zhen, J., Younger, M. A., Yamaguchi, S., Blau, J., Desplan, C., &

774 Sprecher, S. G. (2011). Distinct visual pathways mediate Drosophila larval light avoidance and

775 circadian clock entrainment. *The Journal of Neuroscience : The Official Journal of the Society*

776 *for Neuroscience*, *31*(17), 6527–6534. https://doi.org/10.1523/JNEUROSCI.6165-10.2011

777 Kennedy, T. E., Serafini, T., de la Torre, J. R., & Tessier-Lavigne, M. (1994). Netrins are diffusible

778 chemotropic factors for commissural axons in the embryonic spinal cord. *Cell*, *78*(3), 425–435.

779 https://doi.org/10.1016/0092-8674(94)90421-9

780 Kidd, T., Brose, K., Mitchell, K. J., Fetter, R. D., Tessier-Lavigne, M., Goodman, C. S., & Tear, G.

781 (1998). Roundabout controls axon crossing of the CNS midline and defines a novel subfamily

782 of evolutionarily conserved guidance receptors. *Cell*, *92*(2), 205–215.

783 https://doi.org/10.1016/s0092-8674(00)80915-0

784 Koch, D., Rosoff, W. J., Jiang, J., Geller, H. M., & Urbach, J. S. (2012). Strength in the periphery:

785 growth cone biomechanics and substrate rigidity response in peripheral and central nervous

786 system neurons. *Biophysical Journal*, *102*(3), 452–460. https://doi.org/10.1016/j.bpj.2011.12.025

787 Kolodkin, A. L., & Tessier-Lavigne, M. (2011). Mechanisms and molecules of neuronal wiring: A

788 primer. *Cold Spring Harbor Perspectives in Biology*, *3*(6), 1–14.

789 https://doi.org/10.1101/cshperspect.a001727

790 Lee, T., Lee, A., & Luo, L. (1999). Development of the Drosophila mushroom bodies: sequential

791 generation of three distinct types of neurons from a neuroblast. *Development (Cambridge,*

792 *England)*, *126*(18), 4065–4076. https://doi.org/10.1242/dev.126.18.4065

793 Li, T., Fu, T.-M., Wong, K. K. L., Li, H., Xie, Q., Luginbuhl, D. J., Wagner, M. J., Betzig, E., & Luo,

L. (2021). Cellular bases of olfactory circuit assembly revealed by systematic time-lapse imaging. *Cell*, *184*(20), 5107-5121.e14. https://doi.org/https://doi.org/10.1016/j.cell.2021.08.030

Li, X.-T., Zhou, Q.-S., Yu, Q., Zhao, X., & Liu, Q.-X. (2014). [Current progress in functions of axon guidance molecule Robo and underlying molecular mechanism]. *Sheng li xue bao : [Acta physiologica Sinica]*, *66*(3), 373–385.

Liu, G., Li, W., Wang, L., Kar, A., Guan, K. L., Rao, Y., & Wu, J. Y. (2009). DSCAM functions as a netrin receptor in commissural axon pathfinding. *Proceedings of the National Academy of Sciences of the United States of America*, *106*(8), 2951–2956. https://doi.org/10.1073/pnas.0811083106

Liu, T., Mahesh, G., Houl, J. H., & Hardin, P. E. (2015). Circadian activators are expressed days before they initiate clock function in late pacemaker neurons from Drosophila. *Journal of Neuroscience*, *35*(22), 8662–8671. https://doi.org/10.1523/JNEUROSCI.0250-15.2015

Long, H., Sabatier, C., Ma, L., Plump, A., Yuan, W., Ornitz, D. M., Tamada, A., Murakami, F., Goodman, C. S., & Tessier-Lavigne, M. (2004). Conserved roles for Slit and Robo proteins in midline commissural axon guidance. *Neuron*, *42*(2), 213–223. https://doi.org/10.1016/s0896-6273(04)00179-5

Lowery, L. A., & Vactor, D. Van. (2009). The trip of the tip: understanding the growth cone machinery. *Nature Reviews Molecular Cell Biology*, *10*(5), 332–343. https://doi.org/10.1038/nrm2679

Ly, A., Nikolaev, A., Suresh, G., Zheng, Y., Tessier-Lavigne, M., & Stein, E. (2008). DSCAM Is a Netrin Receptor that Collaborates with DCC in Mediating Turning Responses to Netrin-1. *Cell*, *133*(7), 1241–1254. https://doi.org/10.1016/j.cell.2008.05.030

Martins, L. F., Brambilla, I., Motta, A., de Pretis, S., Bhat, G. P., Badaloni, A., Malpighi, C., Amin, N. D., Imai, F., Almeida, R. D., Yoshida, Y., Pfaff, S. L., & Bonanomi, D. (2022). Motor neurons use push-pull signals to direct vascular remodeling critical for their connectivity. *Neuron*, *110*(24), 4090-4107.e11. https://doi.org/10.1016/j.neuron.2022.09.021

Matthews, B. J., & Grueber, W. B. (2011). Dscam1-mediated self-avoidance counters netrin-dependent targeting of dendrites in drosophila. *Current Biology*, *21*(17), 1480–1487. https://doi.org/10.1016/j.cub.2011.07.040

Mitchell, K. J., Doyle L., J. L., Serafini, T., Kennedy, T. E., Tessier-Lavigne, M., Goodman, C. S., & Dickson, B. J. (1996). Genetic analysis of Netrin genes in Drosophila: Netrins guide CNS

824 commissural axons and peripheral motor axons. *Neuron*, *17*(2), 203–215.
825 https://doi.org/10.1016/S0896-6273(00)80153-1
826 Mortimer, D., Fothergill, T., Pujic, Z., Richards, L. J., & Goodhill, G. J. (2008). Growth cone
827 chemotaxis. *Trends in Neurosciences*, *31*(2), 90–98.
828 https://doi.org/https://doi.org/10.1016/j.tins.2007.11.008
829 Neuhaus-Follini, A., & Bashaw, G. J. (2015). Crossing the embryonic midline: molecular mechanisms
830 regulating axon responsiveness at an intermediate target. *WIREs Developmental Biology*, *4*(4),
831 377–389. https://doi.org/https://doi.org/10.1002/wdev.185
832 Okray, Z., de Esch, C. E. F., Van Esch, H., Devriendt, K., Claeys, A., Yan, J., Verbeeck, J., Froyen, G.,
833 Willemsen, R., de Vrij, F. M. S., & Hassan, B. A. (2015). A novel fragile X syndrome mutation
834 reveals a conserved role for the carboxy-terminus in FMRP localization and function. *EMBO*
835 *Molecular Medicine*, *7*(4), 423–437. https://doi.org/10.15252/emmm.201404576
836 Oliva, C., Soldano, A., Mora, N., De Geest, N., Claeys, A., Erfurth, M. L., Sierralta, J., Ramaekers, A.,
837 Dascenco, D., Ejsmont, R. K., Schmucker, D., Sanchez-Soriano, N., & Hassan, B. A. (2016).
838 Regulation of Drosophila Brain Wiring by Neuropil Interactions via a Slit-Robo-RPTP Signaling
839 Complex. *Developmental Cell*, *39*(2), 267–278. https://doi.org/10.1016/j.devcel.2016.09.028
840 Orioli, D., & Klein, R. (1997). The Eph receptor family: axonal guidance by contact repulsion. *Trends*
841 *in Genetics : TIG*, *13*(9), 354–359. https://doi.org/10.1016/s0168-9525(97)01220-1
842 Pauls, D., Selcho, M., Gendre, N., Stocker, R. F., & Thum, A. S. (2010). Drosophila larvae establish
843 appetitive olfactory memories via mushroom body neurons of embryonic origin. *Journal of*
844 *Neuroscience*, *30*(32), 10655–10666. https://doi.org/10.1523/JNEUROSCI.1281-10.2010
845 Piper, M., Plachez, C., Zalucki, O., Fothergill, T., Goudreau, G., Erzurumlu, R., Gu, C., & Richards, L.
846 J. (2009). Neuropilin 1-Sema Signaling Regulates Crossing of Cingulate Pioneering Axons
847 during Development of the Corpus Callosum. *Cerebral Cortex*, *19*(suppl_1), i11–i21.
848 https://doi.org/10.1093/cercor/bhp027
849 Pirooznia, S. K., Chiu, K., Chan, M. T., Zimmerman, J. E., & Elefant, F. (2012). Epigenetic Regulation
850 of Axonal Growth of Drosophila Pacemaker Cells by Histone Acetyltransferase Tip60 Controls
851 Sleep. *Genetics*, *192*(4), 1327–1345. https://doi.org/10.1534/genetics.112.144667
852 Puñal, V. M., Ahmed, M., Thornton-Kolbe, E. M., & Clowney, E. J. (2021). Untangling the wires:
853 development of sparse, distributed connectivity in the mushroom body calyx. *Cell and Tissue*

Research, *383*(1), 91–112. https://doi.org/10.1007/s00441-020-03386-4

Purohit, A. A., Li, W., Qu, C., Dwyer, T., Shao, Q., Guan, K. L., & Liu, G. (2012). Down syndrome cell adhesion molecule (DSCAM) associates with uncoordinated-5C (UNC5C) in netrin-1-mediated growth cone collapse. *Journal of Biological Chemistry*, *287*(32), 27126–27138. https://doi.org/10.1074/jbc.M112.340174

Reinhard, N., Schubert, F. K., Bertolini, E., Hagedorn, N., Manoli, G., Sekiguchi, M., Yoshii, T., Rieger, D., & Helfrich-Förster, C. (2022). The Neuronal Circuit of the Dorsal Circadian Clock Neurons in Drosophila melanogaster. *Frontiers in Physiology*, *13*, 886432. https://doi.org/10.3389/fphys.2022.886432

Schlichting, M., Richhariya, S., Herndon, N., Ma, D., Xin, J., Lenh, W., Abruzzi, K., & Rosbash, M. (2022). Dopamine and GPCR-mediated modulation of DN1 clock neurons gates the circadian timing of sleep. *Proceedings of the National Academy of Sciences of the United States of America*, *119*(34), e2206066119. https://doi.org/10.1073/pnas.2206066119

Schmucker, D., Clemens, J. C., Shu, H., Worby, C. A., Xiao, J., Muda, M., Dixon, J. E., & Zipursky, S. L. (2000). Drosophila Dscam is an axon guidance receptor exhibiting extraordinary molecular diversity. *Cell*, *101*(6), 671–684. https://doi.org/10.1016/s0092-8674(00)80878-8

Serafini, T., Colamarino, S. A., Leonardo, E. D., Wang, H., Beddington, R., Skarnes, W. C., & Tessier-Lavigne, M. (1996). Netrin-1 is required for commissural axon guidance in the developing vertebrate nervous system. *Cell*, *87*(6), 1001–1014. https://doi.org/10.1016/s0092-8674(00)81795-x

Shields, A. R., Spence, A. C., Yamashita, Y. M., Davies, E. L., & Fuller, M. T. (2014). The actin-binding protein profilin is required for germline stem cell maintenance and germ cell enclosure by somatic cyst cells. *Development*, *141*(1), 73–82. https://doi.org/10.1242/dev.101931

Squarzoni, P., Thion, M. S., & Garel, S. (2015). Neuronal and microglial regulators of cortical wiring: usual and novel guideposts. *Frontiers in Neuroscience*, *9*, 248. https://doi.org/10.3389/fnins.2015.00248

Stoeckli, E T, Sonderegger, P., Pollerberg, G. E., & Landmesser, L. T. (1997). Interference with axonin-1 and NrCAM interactions unmasks a floor-plate activity inhibitory for commissural axons. *Neuron*, *18*(2), 209–221. https://doi.org/10.1016/s0896-6273(00)80262-7

Stoeckli, Esther T. (2018). Understanding axon guidance: are we nearly there yet? *Development*,

884 *145*(10), dev151415. https://doi.org/10.1242/dev.151415

885 Sudarsanam, S., Yaniv, S., Meltzer, H., & Schuldiner, O. (2020). Cofilin regulates axon growth and
886 branching of Drosophila γ-neurons. *Journal of Cell Science*, *133*(8).
887 https://doi.org/10.1242/jcs.232595

888 Suzuki, Y., Kurata, Y., & Sakai, T. (2022). Dorsal–lateral clock neurons modulate consolidation and
889 maintenance of long-term memory in Drosophila. *Genes to Cells*, *27*(4), 266–279.
890 https://doi.org/https://doi.org/10.1111/gtc.12923

891 Unni, D. K., Piper, M., Moldrich, R. X., Gobius, I., Liu, S., Fothergill, T., Donahoo, A.-L. S., Baisden,
892 J. M., Cooper, H. M., & Richards, L. J. (2012). Multiple Slits regulate the development of
893 midline glial populations and the corpus callosum. *Developmental Biology*, *365*(1), 36–49.
894 https://doi.org/https://doi.org/10.1016/j.ydbio.2012.02.004

895 Vitriol, E. A., & Zheng, J. Q. (2012). Growth cone travel in space and time: the cellular ensemble of
896 cytoskeleton, adhesion, and membrane. *Neuron*, *73*(6), 1068–1081.
897 https://doi.org/10.1016/j.neuron.2012.03.005

898 Worby, C. A., Simonson-Leff, N., Clemens, J. C., Kruger, R. P., Muda, M., & Dixon, J. E. (2001). The
899 sorting nexin, DSH3PX1, connects the axonal guidance receptor, Dscam, to the actin
900 cytoskeleton. *The Journal of Biological Chemistry*, *276*(45), 41782–41789.
901 https://doi.org/10.1074/jbc.M107080200

902 Yang, L., Garbe, D. S., & Bashaw, G. J. (2009). A frazzled/DCC-dependent transcriptional switch
903 regulates midline axon guidance. *Science (New York, N.Y.)*, *324*(5929), 944–947.
904 https://doi.org/10.1126/science.1171320

905 Zang, Y., Chaudhari, K., & Bashaw, G. J. (2021). New insights into the molecular mechanisms of axon
906 guidance receptor regulation and signaling. *Current Topics in Developmental Biology*, *142*,
907 147–196. https://doi.org/10.1016/bs.ctdb.2020.11.008

908 Zhan, X. L., Clemens, J. C., Neves, G., Hattori, D., Flanagan, J. J., Hummel, T., Vasconcelos, M. L.,
909 Chess, A., & Zipursky, S. L. (2004). Analysis of Dscam diversity in regulating axon guidance in
910 Drosophila mushroom bodies. *Neuron*, *43*(5), 673–686.
911 https://doi.org/10.1016/j.neuron.2004.07.020

912 Zhang, Z., So, K., Peterson, R., Bauer, M., Ng, H., Zhang, Y., Kim, J. H., Kidd, T., & Miura, P. (2019).
913 Elav-Mediated Exon Skipping and Alternative Polyadenylation of the Dscam1 Gene Are

914 Required for Axon Outgrowth. *Cell Reports*, *27*(13), 3808-3817.e7.

915 https://doi.org/10.1016/j.celrep.2019.05.083

916

Figure 1

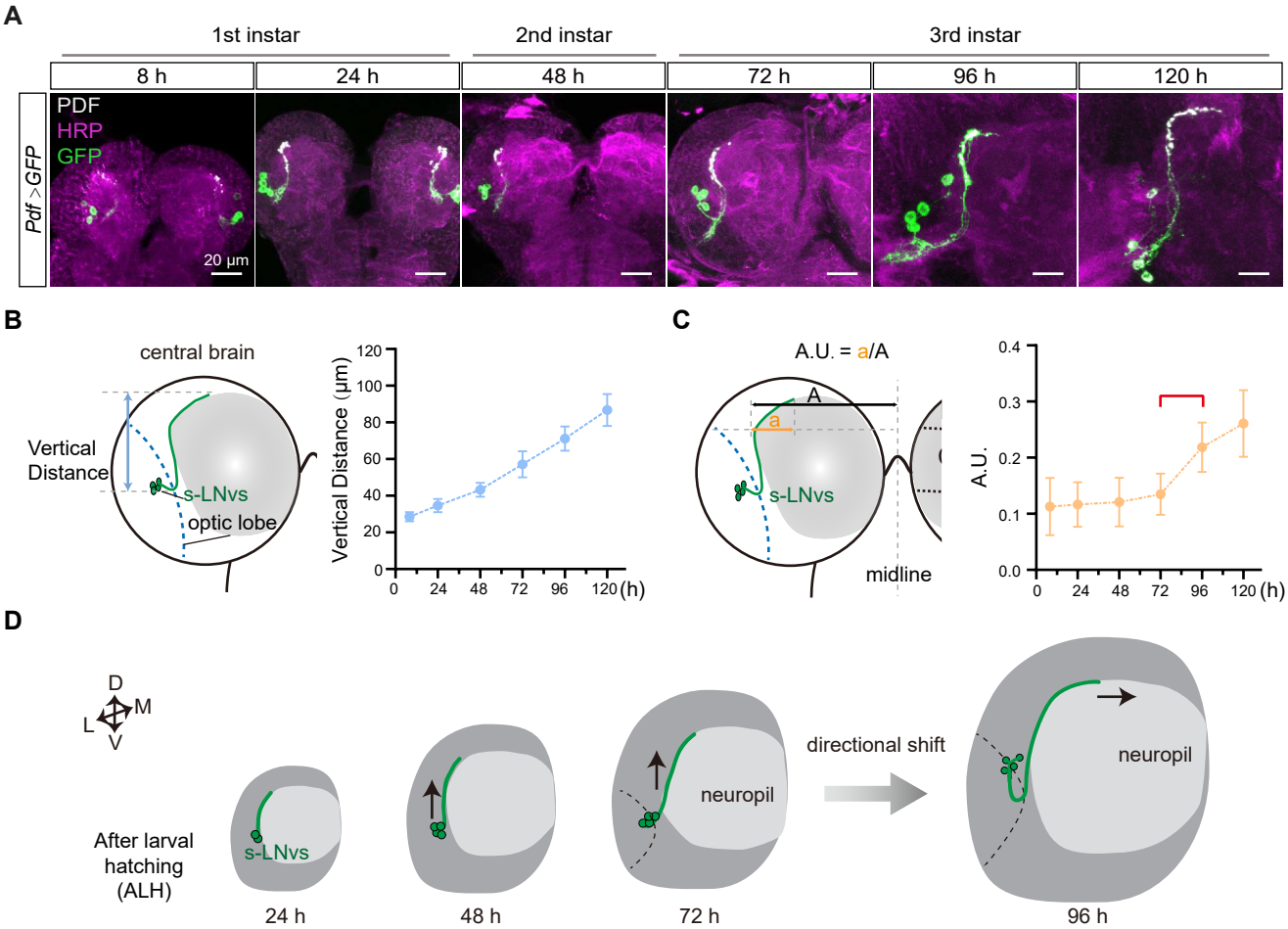
A
1st instar
2nd instar
3rd instar
8 h
24 h
48 h
72 h
96 h
120 h
Pdf > GFP
PDF
HRP
GFP
20 μm
B
central brain
Vertical Distance
s-LNvs
optic lobe
Vertical Distance (μm)
120
100
80
60
40
20
0
0
24
48
72
96
120 (h)
C
A.U. = a/A
A
a
s-LNvs
midline
A.U.
0.4
0.3
0.2
0.1
0.0
0
24
48
72
96
120 (h)
D
D
M
L
V
After larval hatching (ALH)
s-LNvs
24 h
48 h
neuropil
72 h
directional shift
neuropil
96 h

Figure 2

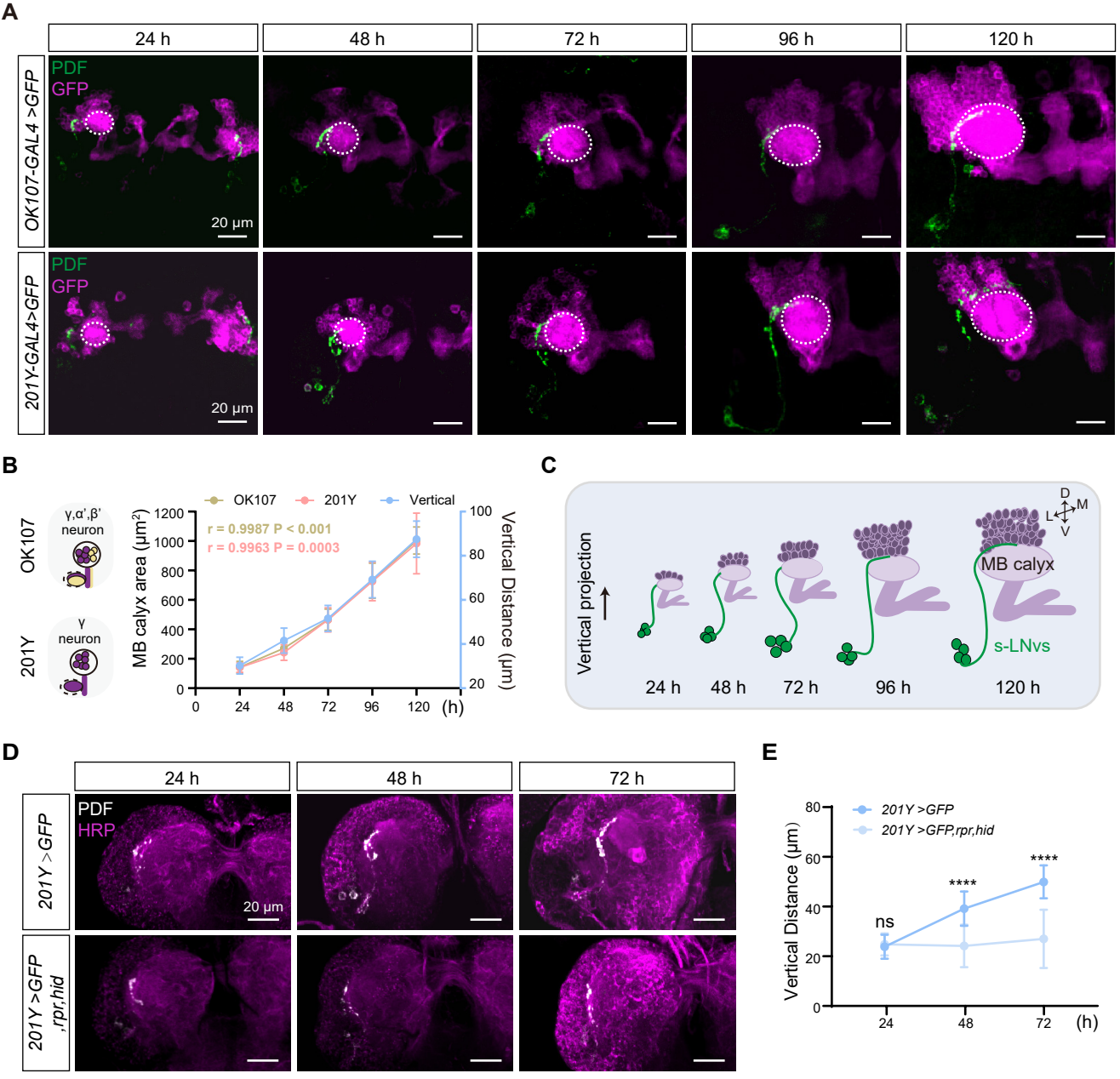
A
24 h
48 h
72 h
96 h
120 h
OK107-GAL4 >GFP
201Y-GAL4>GFP
PDF
GFP
20 μm
B
OK107
γ,α',β' neuron
201Y
γ neuron
OK107
201Y
Vertical
r = 0.9987 P < 0.001
r = 0.9963 P = 0.0003
MB calyx area (μm²)
Vertical Distance (μm)
(h)
C
Vertical projection
D
M
L
V
MB calyx
s-LNvs
24 h
48 h
72 h
96 h
120 h
D
24 h
48 h
72 h
201Y >GFP
201Y >GFP ,rpr,hid
PDF
HRP
20 μm
E
201Y >GFP
201Y >GFP,rpr,hid
Vertical Distance (μm)
ns
****
****
(h)

Figure 3

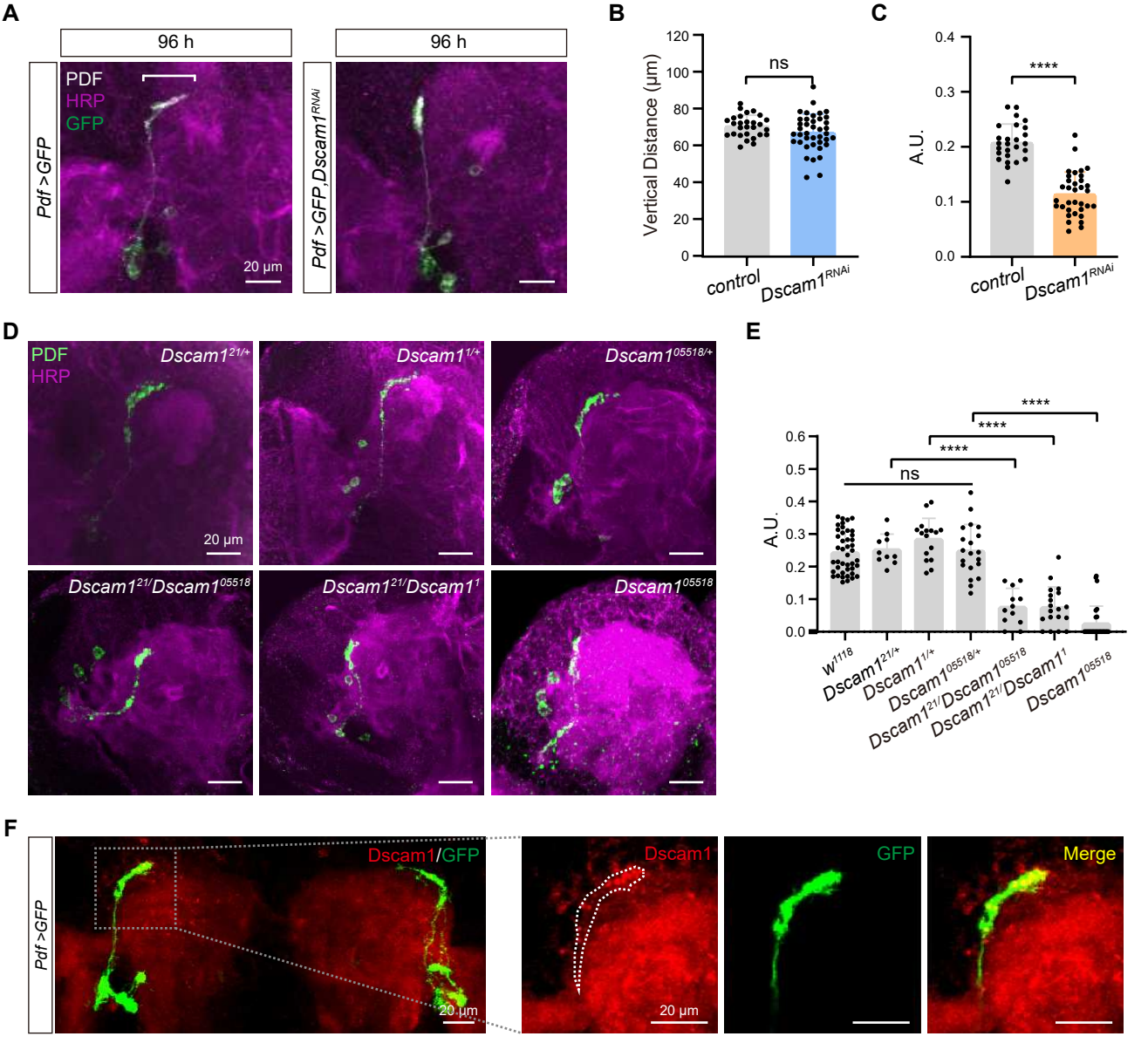
A
96 h
96 h
Pdf >GFP
Pdf >GFP,Dscam1RNAi
PDF
HRP
GFP
20 µm
B
Vertical Distance (µm)
ns
control
Dscam1RNAi
C
A.U.
****
control
Dscam1RNAi
D
PDF
HRP
Dscam121/+
Dscam11/+
Dscam105518/+
Dscam121/Dscam105518
Dscam121/Dscam11
Dscam105518
20 µm
E
A.U.
ns
****
****
****
w1118
Dscam121/+
Dscam11/+
Dscam105518/+
Dscam121/Dscam105518
Dscam121/Dscam11
Dscam105518
F
Pdf >GFP
Dscam1/GFP
Dscam1
GFP
Merge
20 µm
20 µm

Figure 4

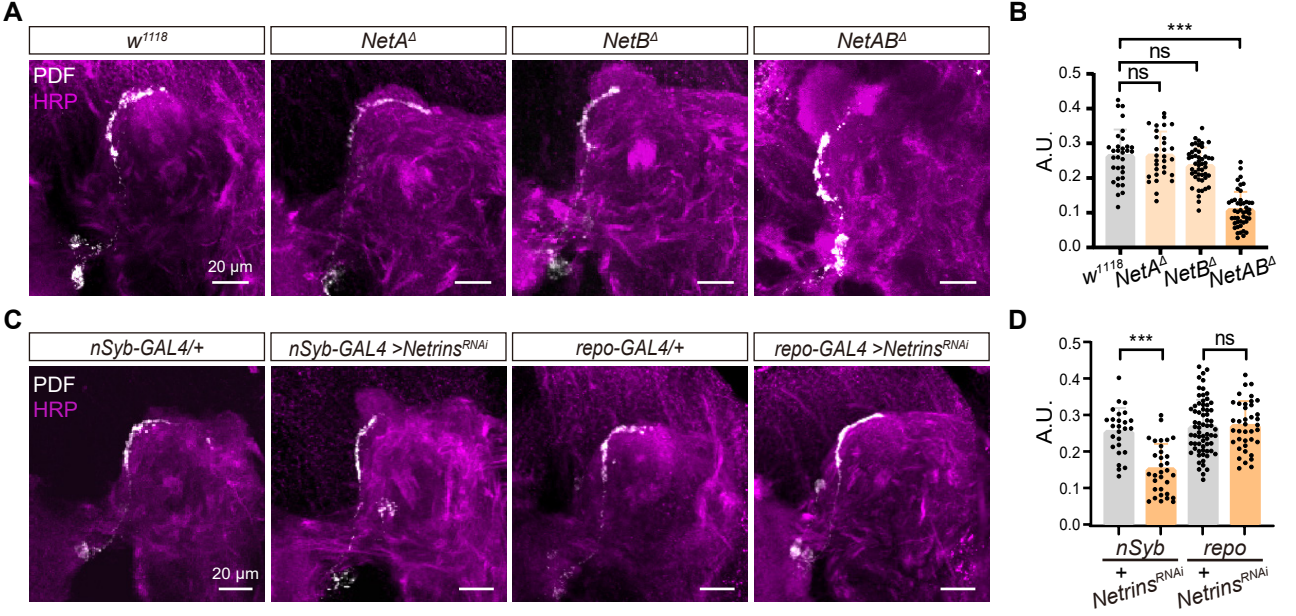
A
w1118
NetAΔ
NetBΔ
NetABΔ
PDF
HRP
20 µm
B
***
ns
ns
A.U.
0.5
0.4
0.3
0.2
0.1
0.0
w1118
NetAΔ
NetBΔ
NetABΔ
C
nSyb-GAL4/+
nSyb-GAL4 >NetrinsRNAi
repo-GAL4/+
repo-GAL4 >NetrinsRNAi
PDF
HRP
20 µm
D
***
ns
A.U.
0.5
0.4
0.3
0.2
0.1
0.0
nSyb
repo
+
NetrinsRNAi
+
NetrinsRNAi

Figure 5

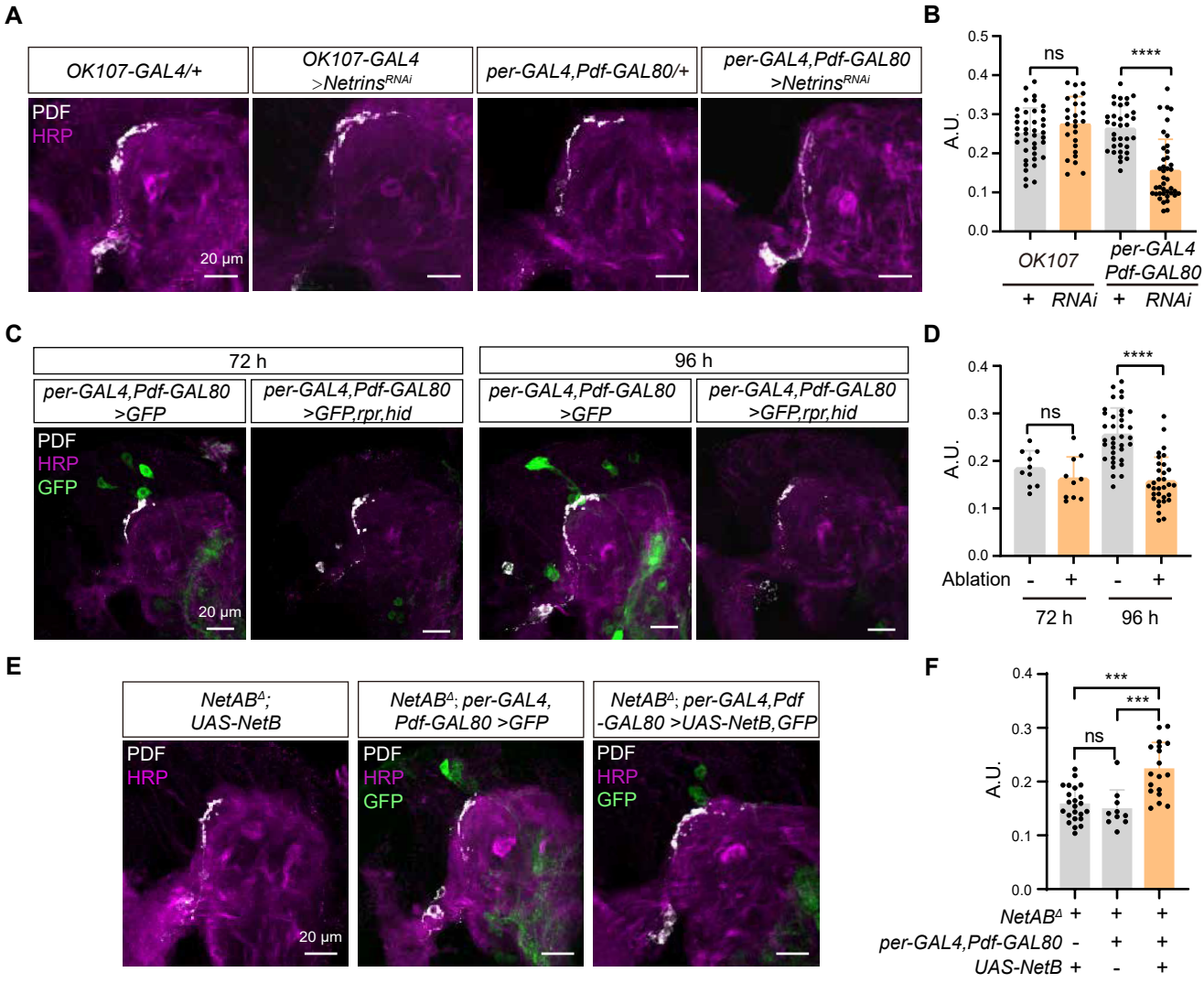
A
OK107-GAL4/+
OK107-GAL4 >Netrins^RNAi
per-GAL4,Pdf-GAL80/+
per-GAL4,Pdf-GAL80 >Netrins^RNAi
PDF
HRP
20 µm
B
ns
****
A.U.
0.5
0.4
0.3
0.2
0.1
0.0
OK107
per-GAL4 Pdf-GAL80
+ RNAi + RNAi
C
72 h
96 h
per-GAL4,Pdf-GAL80 >GFP
per-GAL4,Pdf-GAL80 >GFP,rpr,hid
per-GAL4,Pdf-GAL80 >GFP
per-GAL4,Pdf-GAL80 >GFP,rpr,hid
PDF
HRP
GFP
20 µm
D
ns
****
A.U.
0.4
0.3
0.2
0.1
0.0
Ablation - + - +
72 h
96 h
E
NetAB^Δ; UAS-NetB
NetAB^Δ; per-GAL4, Pdf-GAL80 >GFP
NetAB^Δ; per-GAL4,Pdf -GAL80 >UAS-NetB,GFP
PDF
HRP
GFP
20 µm
F
***
***
ns
A.U.
0.4
0.3
0.2
0.1
0.0
NetAB^Δ + + +
per-GAL4,Pdf-GAL80 - + +
UAS-NetB + - +

Figure 6

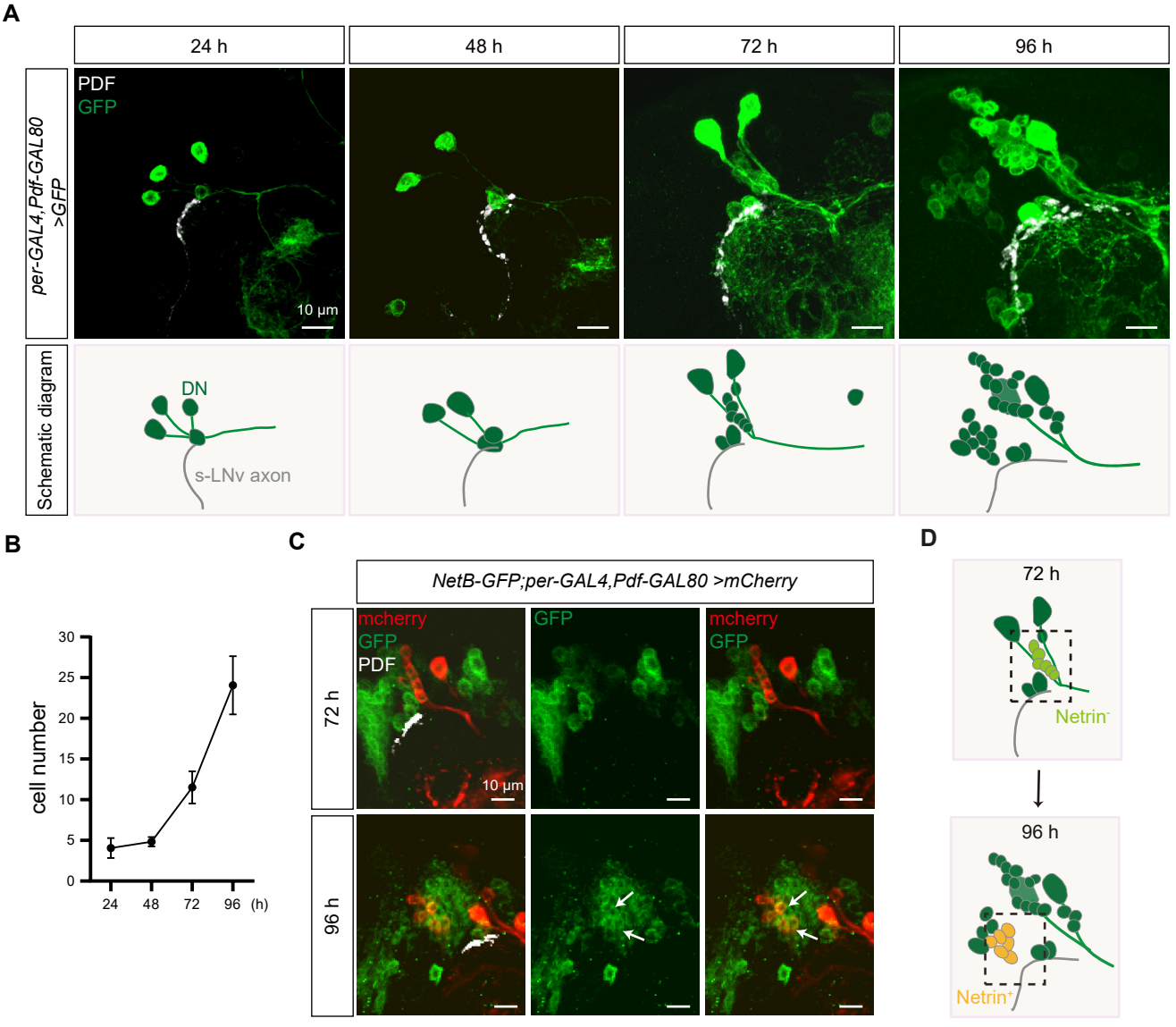
A
24 h
48 h
72 h
96 h
per-GAL4,Pdf-GAL80 >GFP
PDF
GFP
10 μm
Schematic diagram
DN
s-LNv axon
B
cell number
30
25
20
15
10
5
0
24
48
72
96 (h)
C
NetB-GFP;per-GAL4,Pdf-GAL80 >mCherry
72 h
96 h
mcherry
GFP
PDF
10 μm
D
72 h
Netrin-
96 h
Netrin+

Figure 7

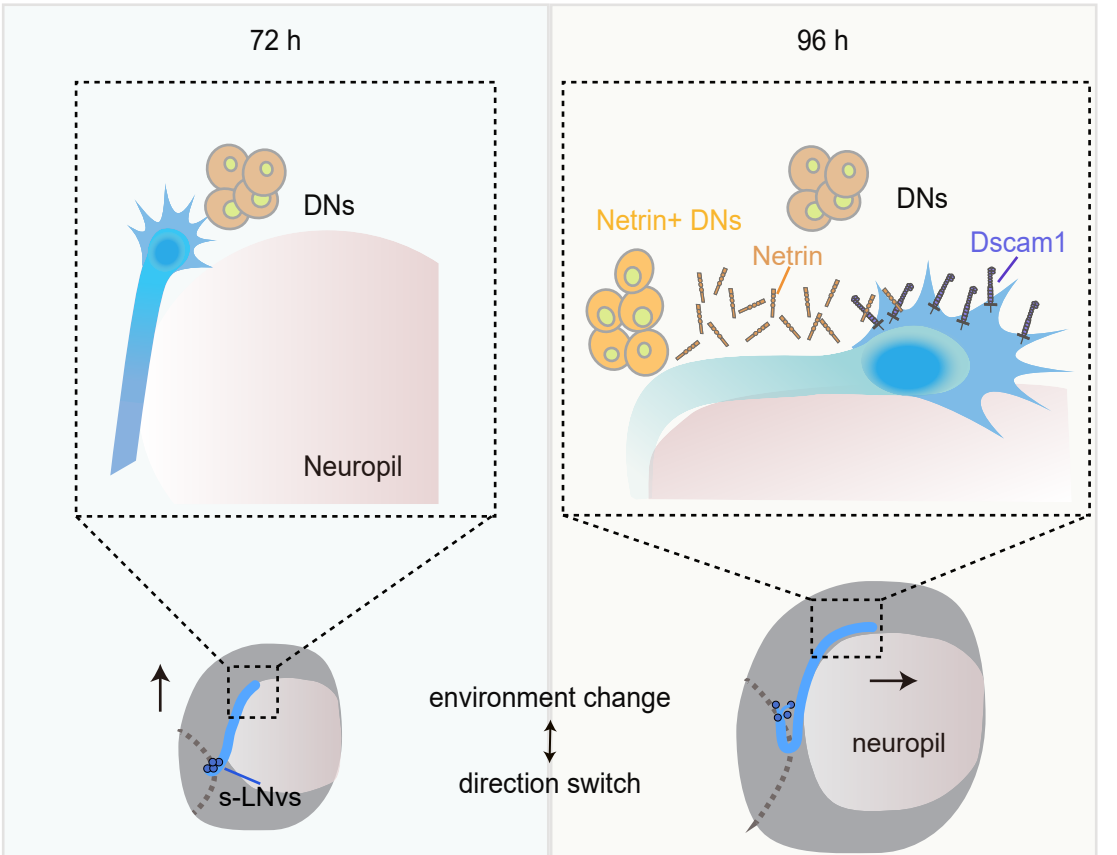
72 h
96 h
DNs
Neuropil
Netrin+ DNs
DNs
Netrin
Dscam1
s-LNvs
environment change
direction switch
neuropil